Studies into electrochemical hydrogenation reactions using molecular catalysts

Verbeek, S.

Chapter 4

Synthesis and application of a cobaltocenium complex for mediated electro-synthesis

The cyclopentadienyl ligand HCp^N containing a pendant 2-picolyl group (HCp^N = $C_5H_5CH_2C_5H_4N$) was employed for the synthesis of the new cobaltocenium compound $[Co^{III}(Cp^{NH})_2](PF_6)_3$. The redox properties of this compound were investigated using cyclic voltammetry in acetonitrile. The Co^{III}/Co^{II} redox couple of $[Co^{III}(Cp^{NH})_2](PF_6)_3$ under argon atmosphere is reversible, but after several scans the redox features of $[Co^{III}(Cp^N)_2]^+$ appeared. The redox chemistry of $[Co^{III}(Cp^N)_2]PF_6$ was also investigated and showed a significant shift in the reduction potential ($E_{1/2}$ = –1.39 V and –1.14 V vs $Fc^{+/0}$, respectively for $[Co^{III}(Cp^N)_2]PF_6$ and $[Co^{III}(Cp^{NH})_2](PF_6)_3$). The potential application of $[Co^{III}(Cp^{NH})_2](PF_6)_3$ as a PCET mediator was investigated for the electrocatalytic semi-hydrogenation of alkynes with a nickel electrocatalyst. Electrocatalytic semi-hydrogenation experiments were conducted using the substrate methyl 3-phenyl-2-propynoate and p-toluenesulfonic acid (p-HOTs) as the proton source, with $[Co^{III}(Cp^{NH})_2](PF_6)_3$ as mediator for the commercially available nickel complex $[Ni^{II}(dppe)Cl_2]$ (dppe = 1,2-bis(diphenylphosphino)ethane) as electrocatalyst. $[Ni^{II}(dppe)Cl_2]$ revealed to be more effective for electrocatalytic semi-hydrogenation of methyl 3-phenyl-2-propynoate in absence of the mediator.

4.1 Introduction

The synthesis of alkenes can be achieved through several methods.[1] One such method is the semi-hydrogenation reaction of alkynes, commonly catalyzed by the Lindlar's catalyst.[2] The Lindlar's catalyst and several heterogeneous and homogeneous catalysts catalyze the semi-hydrogenation reaction in the presence of dihydrogen gas.[3] An alternative approach is the electrocatalytic reduction of alkynes in the presence of protons; this approach does not require dihydrogen gas, as described in Chapter 3.

The homogeneous nickel catalyst [Ni^{II}(neocuproine)Cl_2] discussed in Chapter 3 is capable of electrochemical semi-hydrogenation of alkynes in the presence of benzoic acid. Nitrogen-based ligands, like 2,2'-bipyridine, are often employed in electrochemical reduction reactions since electrons can be stored in these aromatic ligands.[4] However, such nitrogen-based ligands are not commonly used in homogeneous (transfer) hydrogenation reactions with nickel complexes. Instead phosphine-based ligands are preferred,[5] as they are better at stabilizing nickel(0) intermediates based on their soft-donor ability.[6] Phosphine-based nickel complexes are also efficient catalysts for the electrochemical hydrogen-evolution reaction (HER).[7,8] In the HER a nickel-hydride intermediate is generated, which is also a crucial intermediate for hydrogenation reactions.[9] In order to semi-hydrogenate alkynes with an electrochemically generated nickel-hydride intermediate it is essential to optimize the reaction so that HER is suppressed and semi-hydrogenation is promoted.[10,11]

A key difference between phosphine-based nickel(II) complexes that have been studied thus far for HER and hydrogenation reactions is the number of phosphine ligands coordinated to the nickel(II) center. In HER catalysts the nickel(II) center is commonly coordinated by two bidentate phosphine ligands, resulting in a 16-electron, square-planar complex of the general formula $[Ni^{II}(P_2)_2]^{2+}$ (P_2 = bidentate phosphine ligand).[8] In a typical catalyst for hydrogenation reactions, the nickel(II) center is coordinated by phosphine donor atoms and two (labile) anionic ligands, in compounds with the general formula $[Ni^{II}(P_2)(X)_2]$ (where P_2 = two monodentate or one bidentate phosphine ligand, and X = anionic ligand). The presence of labile anionic ligands is essential to provide potential binding sites for the substrate.[5]

Electrochemical reduction of $[Ni^{II}(P_2)_2]^{2+}$ is generally a reversible process,[12,13] illustrating that stable nickel(I) and nickel(0) intermediates are formed. The electrochemical reduction of $[Ni^{II}(P_2)(X)_2]$ is often more complicated as formation of nickel(I) and nickel(0) intermediates often triggers a series of disproportionation and comproportionation reactions.[14–16] The electrochemical generation of a nickel(0) intermediate is necessary for the generation of a nickel(II)-hydride, which can be produced upon protonation.[7] Due to the negative operating potential being applied, the electrochemically generated nickel(II)-hydride intermediate may possibly be reduced to a nickel(I)-hydride compound,[17] which is a more powerful hydride donor. From electrochemical HER studies it is known that nickel(I)-hydrides quickly react with protons to form H_2, whereas nickel(II)-hydrides are less reactive with protons.[8] The nickel(I) and nickel(II)-hydride compounds may both participate in hydrogenation reactions of alkynes.[10] In order to avoid formation of nickel(I)-hydride intermediates that are active in

HER, another method is necessary to form the desired nickel(II)-hydride compounds for alkyne hydrogenation. An indirect reduction of the electrocatalyst to form the nickel(II)-hydride can be achieved through a process called proton-coupled electron transfer (PCET).[18,19] A PCET mediator can promote formation of the desired nickel(II)-hydride at a potential that is high enough to avoid reduction to the nickel(I)-hydride.

A promising class of PCET mediators are metallocenes, such as ferrocene and cobaltocene.[20–28] Cobaltocene $[Co^{II}(\eta^5\text{-}C_5H_5)_2]$ is a one-electron reducing agent, and is a promising candidate for PCET. Cobaltocene can be protonated by strong acids to form $[Co^{II}(\eta^4\text{-}C_5H_6)(\eta^5\text{-}C_5H_5)]^+$, which is reported to release H_2 with the formation of $[Co^{III}(\eta^5\text{-}C_5H_5)_2]^+$.[29] This process may lead to inefficient PCET mediation to the electrocatalyst for semi-hydrogenation. It has been reported that the permethylated cobaltocene compound $[Co^{II}(\eta^5\text{-}C_5Me_5)]$ operates in a similar fashion to form $[Co^{II}(\eta^4\text{-}C_5Me_5H)(\eta^5\text{-}C_5Me_5)]^+$, which then acts as a hydrogen-atom transfer (HAT) reagent to facilitate reduction of dinitrogen to ammonia, catalyzed by an iron complex.[30,31]

Another report describes a cobaltocenium complex with an aniline substituent $[1H]^{2+}$ (Figure 4.1).[32] Complex $[1H]^{2+}$ was employed as mediator for PCET in combination with nickel or cobalt compounds bearing diphosphine ligands for the electrocatalytic reduction of methyl 3-phenyl-2-propynoate.[32] The proposed mechanism for PCET mediated reduction of methyl

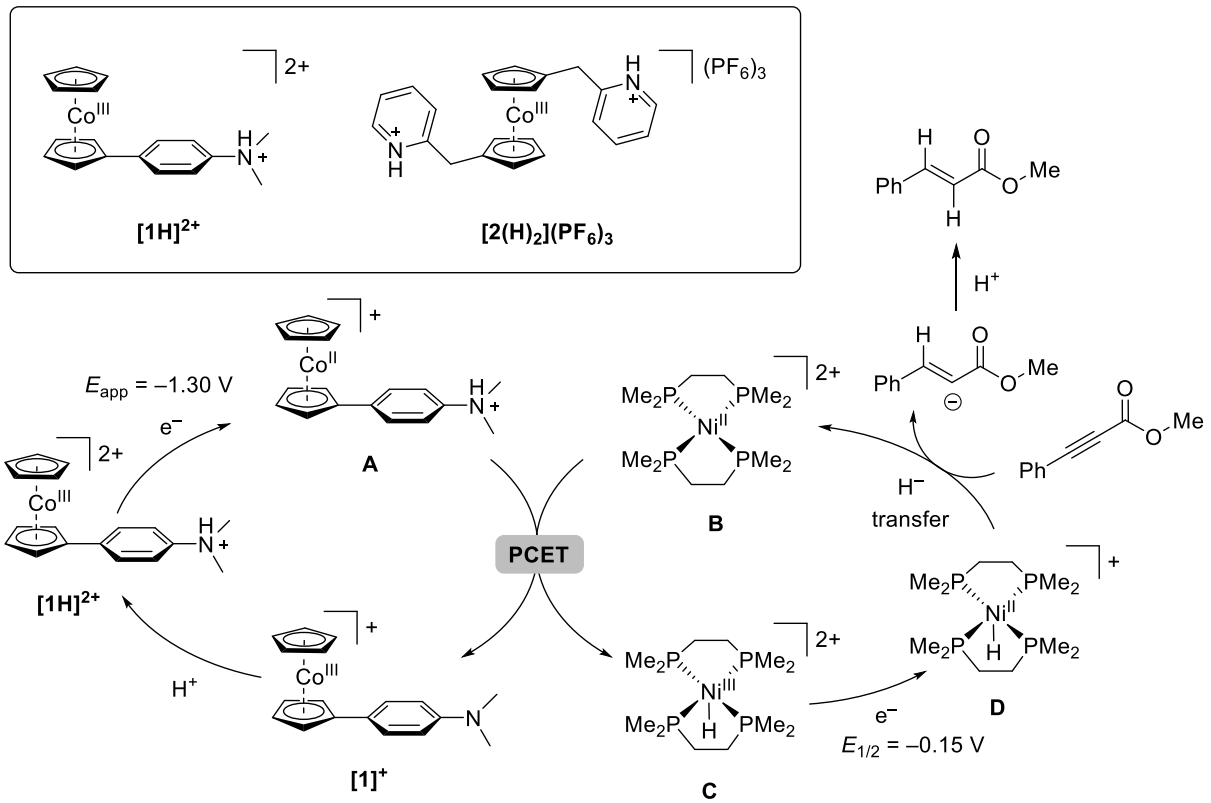

Figure 4.1. (Inset) Schematic representations of cobaltocenium complex $[1H]^{2+}$ reported by Peters,[32] and $[2(H)_2](PF_6)_3$ reported in this Chapter. (Bottom) Proposed mechanism for the hydrogenation reaction performed with $[1H]^{2+}$ as reported by Peters.[32]

3-phenyl-2-propynoate by $[1]^+$ and $[Ni^{II}(dmpe)_2]^{2+}$ is given in Figure 4.1. Through the use of complex A (generated from $[1]^+$) as PCET mediator electrocatalytic HER was suppressed.[32] Interestingly, Peters reported that nickel complexes bearing only one diphosphine ligand, such as $[Ni^{II}(dppe)Cl_2]$ (dppe = 1,2-bis(diphenylphosphino)ethane) and $[Ni^{II}(dppp)Cl_2]$ (dppp = 1,2-bis(diphenylphosphino)propane) may also be employed as electrocatalyst for semi-hydrogenation of methyl 3-phenyl-2-propynoate with $[1]^+$.[32]

In this Chapter a study is described on the use of a new cobaltocene compound as potential PCET mediator in the electrocatalytic semi-hydrogenation of alkynes with nickel-based electrocatalysts. Cobaltocenium compound $[2(H)_2](PF_6)_3$ (Figure 4.1) was synthesized and characterized starting from 2-picolylcyclopentadiene (HCp^N = $C_5H_5CH_2C_5H_4N$). As the pyridine moiety is readily protonated (pK_a = 12.53 of pyridinium in MeCN),[33] it may act as a proton shuttle in electrocatalyzed reactions,[33,34] and it is envisioned that $[2(H)_2](PF_6)_3$ may act as a PCET mediator. $[2(H)_2](PF_6)_3$ was studied with cyclic voltammetry (CV) in the presence of *p*-toluenesulfonic acid (*p*-HOTs) as well as *p*-cyanoanilinium tetrafluoridoborate (pK_a values of 8.6 and 7 in MeCN respectively).[33] Experiments were conducted for electrocatalytic semi-hydrogenation of methyl 3-phenyl-2-propynoate using *p*-HOTs as the proton source, $[2(H)_2](PF_6)_3$ as PCET mediator and commercially available $[Ni^{II}(dppe)Cl_2]$ as electrocatalyst.

4.2 Results and discussion

4.2.1 Synthesis and characterization

The lithium salt of the ligand 2-picolylcyclopentadiene $LiCp^N$ was synthesized according to a reported procedure (Scheme 4.1).[34–36] The orange lithium salt of the ligand was obtained in an overall yield of 20%, which was slightly lower than reported.[36] The product was analyzed with ^1H NMR spectroscopy and considered to be pure enough for further use (Figure A.4.2).

$LiCp^N$ was reacted in a 2:1 ratio with anhydrous $CoCl_2$ in conditions reported for the synthesis of cobaltocene (Scheme 4.1).[37,38] The Co(II) compound $[Co^{II}(Cp^N)_2]$ could not be isolated, due to its oxidation sensitivity and its relatively high solubility in non-polar solvents. Therefore, the reaction mixture was treated with H_2O_2 and air was bubbled through the solution to obtain the stable Co(III) complex. The cationic Co(III) complex is more soluble in water and can thus be readily separated from any unreacted ligand in the reaction mixture. Recrystallization of the crude material from chloroform yielded pure [2]Cl as confirmed with ^1H NMR spectroscopy (Figure A.4.3) and mass analysis (Figure A.4.4). However, as the compound was obtained as a viscous oil, the chloride counter ion was exchanged for PF_6^-. Compound $[2]PF_6$ was obtained as a yellow solid from a reaction of [2]Cl with $AgPF_6$ in MeCN in a yield of 23%.

$[2]PF_6$ was characterized with ^1H, ^{13}C and ^{31}P NMR spectroscopy (Figure A.4.5-6) and mass spectrometry (Figure A.4.7). Whilst $LiCp^N$ shows one singlet at 5.19 ppm for the cyclopentadienyl protons, the NMR spectrum of $[2]PF_6$ shows two pseudo-triplets at 5.72 and 5.68 ppm, similar to a related compound with the ligand

((dimethylamino)ethyl)cyclopentadienyl.[39] Similar splitting of the cyclopentadienyl protons has been reported for $[Fe(Cp^N)_2]$.[40] Mass spectra of $[2]PF_6$ showed the predicted major peak for $[2]^+$ with an *m/z* of 371.4.

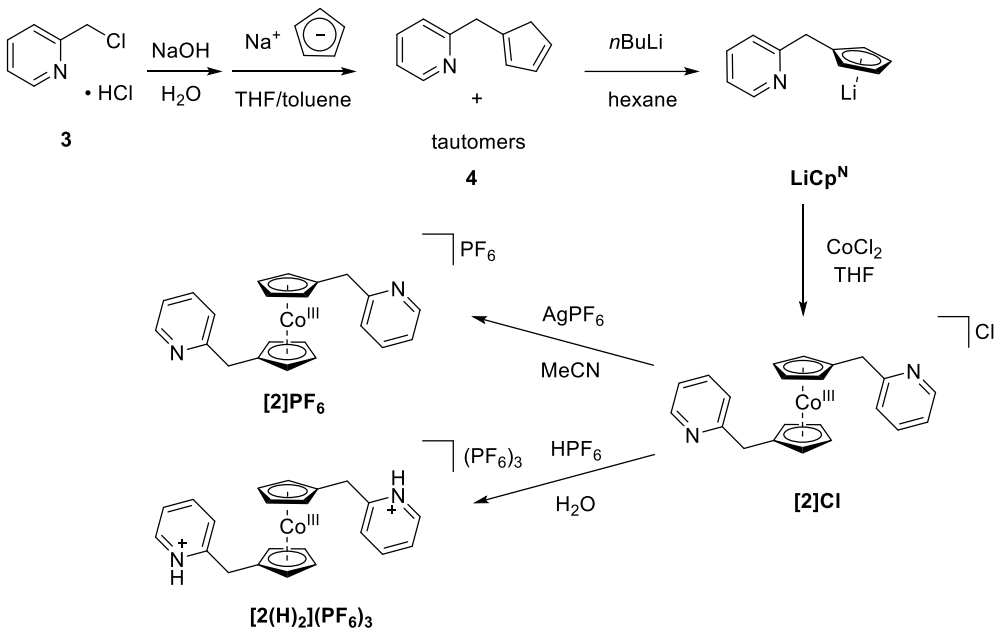

Scheme 4.1. Synthesis scheme of the ligand $LiCp^N$ and complexation with $CoCl_2$ to form [2]Cl and final complexes $[2]PF_6$ and $[2(H)_2](PF_6)_3$.

Protonated compound $[2(H)_2](PF_6)_3$ was obtained from [2]Cl in H_2O upon addition of more than 3 eq. HPF_6 (55 wt.%); overnight storage of the reaction mixture in the refrigerator resulted in a yellow powder that was analytically pure. $[2(H)_2](PF_6)_3$ was characterized with NMR and ESI-MS (Figure A.4.8-12) and single crystal X-ray diffraction. Mass analysis of $[2(H)_2](PF_6)_3$ showed a dominant peak with *m/z* of 371.1, assigned to $[2]^+$ (Figure A.4.12); peaks for $[2+H]^{2+}$ or $[2(H)_2]^{3+}$ were not observed. Elemental analysis of the product was in accordance with $[2(H)_2](PF_6)_3$, in agreement with protonation of both pyridine groups. The UV-vis spectrum of $[2(H)_2](PF_6)_3$ in MeCN (Figure A.4.13) shows an intense peak at 275 nm and two shoulders at 340 nm and 420 nm. The intense peak at 275 nm is ascribed to a ligand-to-metal charge transfer (LMCT) transition, which is slightly redshifted compared to that of $[Co^{III}(\eta^5\text{-}C_5H_5)_2]^+$ (262 nm).[41]

4.2.2 Description of structure

A projection of the structure of the complex cation in $[2(H)_2](PF_6)_3$ is shown in Figure 4.2, the crystal packing is shown in Figure A.4.15, and the crystal data are given in Table A.4.1. $[2(H)_2](PF_6)_3$ crystallizes in the triclinic space group $P\bar{1}$, with the cobalt center located at one site of inversion symmetry. The molecular structure of the cation is like those of most metallocenes, with the metal ion "sandwiched" between two cyclopentadienyl ligands. The structure of $[2(H)_2](PF_6)_3$ comprises one Co(III) ion coordinated to two cyclopentadienyl ligands, each with a 2-picolyl side chain of which the nitrogen atom is protonated, and three PF_6^- anions. The distances between the carbon atoms of the cyclopentadienyl rings and the

cobalt center are found in the range of 2.011 – 2.040 Å, similar to other Co(III)-cyclopentadienyl complexes (2.024 – 2.036 Å).[39,42] The distance of the center of the cyclopentadienyl rings to the cobalt center is 1.63 Å. The cobalt atom is located at one inversion center, and hence there is a staggered configuration of the Cp rings and causes the pyridylmethyl groups to point in opposite directions..

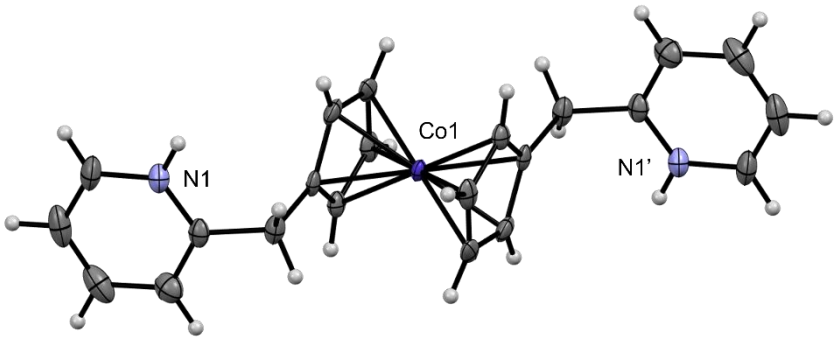

Figure 4.2. Displacement ellipsoid plot (50% probability level) of the cation $[2(H)_2]^{3+}$ at 110(2) K. The PF_6^- counter ions have been omitted for clarity.

4.2.3 Electrochemistry

4.2.3.1 Cyclic voltammetry of $[2(H)_2](PF_6)_3$ in absence of acids

The electrochemical behavior of $[2]PF_6$ and $[2(H)_2](PF_6)_3$ was explored using CV in MeCN solutions containing tetrabutylammonium hexafluoridophosphate (nBu_4NPF_6 0.1 M) as electrolyte and using a glassy carbon (GC) or boron-doped diamond (BDD) working electrode. The two complexes reveal different redox couples for their Co^{III}/Co^{II} redox event, related to the protonation state of the pyridine moieties and the charge of the cation. Understandably, reduction of the cobalt center in $[2]PF_6$ occurs at more negative potentials than for $[2(H)_2](PF_6)_3$ ($E_{1/2}$ = –1.39 V and –1.14 V vs $Fc^{+/0}$, respectively; Figure 4.3). The

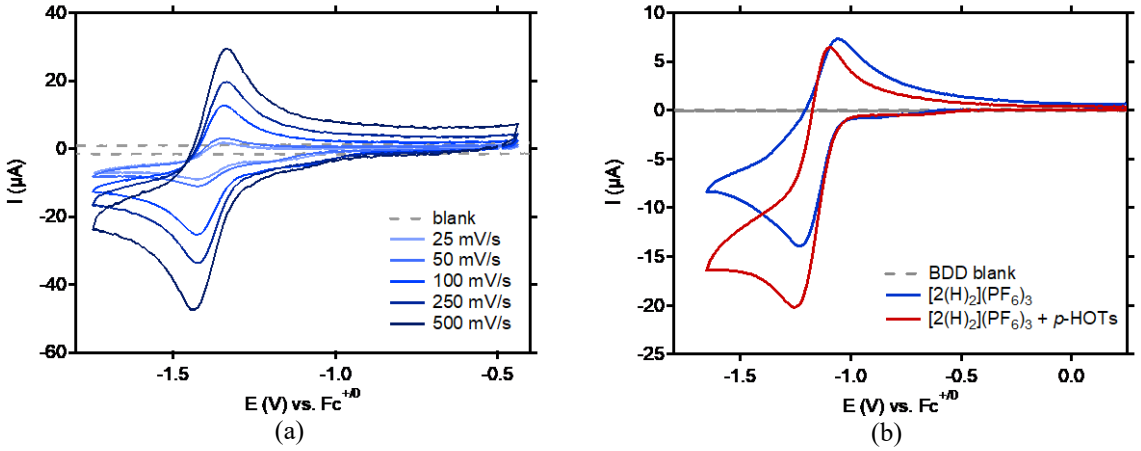

Figure 4.3. (a) Cyclic voltammograms of $[2]PF_6$ (1.0 mM) in 0.1 M nBu_4NPF_6 in MeCN with a GC working electrode (WE), gold wire counter electrode (CE) and Ag/AgCl reference electrode (RE), externally referenced to the $Fc^{+/0}$ redox couple, at a variable scan rate of 25; 50; 100; 250 and 500 mV s^{-1} (light to dark blue). (b) Cyclic voltammograms of $[2(H)_2](PF_6)_3$ in 0.1 M nBu_4NPF_6 in MeCN with a BDD WE, gold wire CE and Ag/AgCl RE, externally referenced to the $Fc^{+/0}$ redox couple, at a fixed scan rate of 100 mV s^{-1}. Complex in absence (blue) and presence (red) of *p*-HOTs•H_2O (2.5 mM).

peak current in the cyclic voltammograms of $[2]PF_6$ increased linearly with increasing scan-rates from 25 to 500 mV s^{-1} (Figure 4.3a), indicating freely diffusing, homogeneous species. The difference in redox potential of 250 mV for the di-protonated and non-protonated complex is similar to that reported for the aniline-substituted cobaltocene complex $[1]^+$ and its mono-protonated form $[1H]^{2+}$ in MeCN/dimethoxyethane (3:1) ($E_{1/2}$ = –1.35 V and –1.21 V vs $Fc^{+/0}$, respectively).[32,42,43] The Co^{III}/Co^{II} redox reaction of cobaltocene $[Co^{II}(\eta^5\text{-}C_5H_5)_2]$ occurs at $E_{1/2}$ of –1.33 V vs $Fc^{+/0}$, indicating that the 2-methylpyridine or aniline substituents at the cyclopentadienyl ring do not exert a significant effect on the electron density at the metal center. The cyclic voltammograms of $[2(H)_2](PF_6)_3$ in MeCN showed loss of reversibility of the Co^{III}/Co^{II} redox couple over several cycles of the cyclic voltammogram (Figure A.4.16) with the gradual appearance of the redox event for $[2]PF_6$ indicating loss of protons upon reduction, which is attributed to formation of dihydrogen gas.

4.2.3.2 Cyclic voltammetry of $[2(H)_2](PF_6)_3$ in presence of acids

Reversibility of the Co^{III}/Co^{II} redox couple of $[2(H)_2](PF_6)_3$ is retained in presence of a small amount of *p*-HOTs (Figure 4.3b), and an increase in current is observed. The cathodic current further increases with higher *p*-HOTs concentrations, and the event becomes irreversible above 10 mM of *p*-HOTs (Figure 4.4a). The addition of increasing amounts of *p*-HOTs resulted in a catalytic wave attributed to the generation of dihydrogen gas, likely in a bimolecular fashion.[29] The reduction of $[2(H)_2](PF_6)_3$ in the presence of *p*-cyanoanilinium tetrafluoridoborate was also recorded with a GC electrode. The current of the Co^{III}/Co^{II} reduction also increases upon addition of the slightly stronger acid *p*-cyanoanilinium tetrafluoridoborate, but this increase is not linear with acid concentration and the redox event becomes less reversible (Figure 4.4b). The ill-defined behavior of the catalytic current may be attributed to interactions of the quaternary pyridinium groups with the GC electrode.[33]

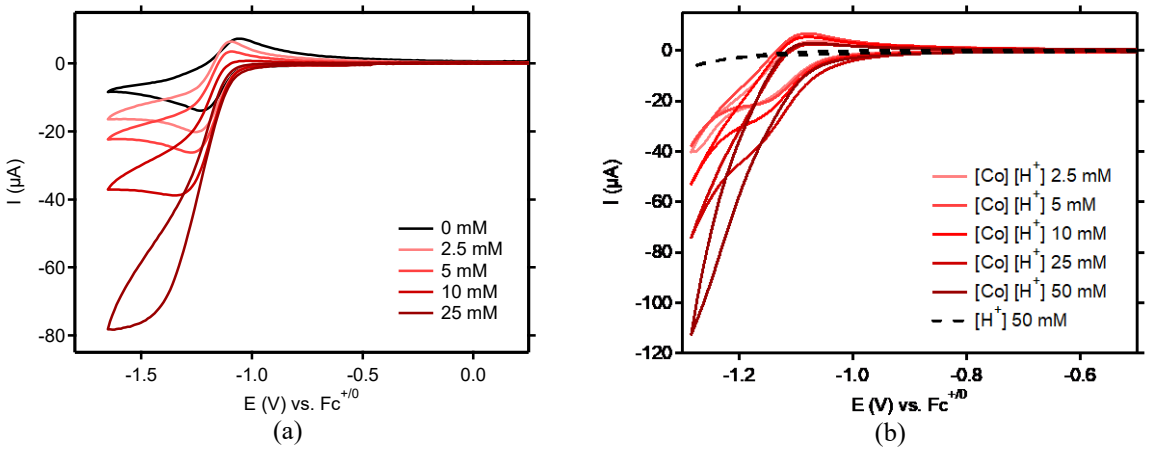

Figure 4.4. (a) Cyclic voltammograms of $[2(H)_2](PF_6)_3$ (1.0 mM, black) in 0.1 M nBu_4NPF_6 in MeCN with a BDD WE, gold wire CE and Ag/AgCl RE externally referenced to the $Fc^{+/0}$ redox couple, at a scan rate of 100 mV s^{-1}, with increasing amounts of *p*-HOTs•H_2O (2.5; 5; 10 and 25 mM, light red – dark red). (b) Cyclic voltammograms of $[2(H)_2](PF_6)_3$ (1.0 mM) in 0.1 M nBu_4NPF_6 in MeCN with a GC WE, gold wire CE and Ag/AgCl RE externally referenced to the $Fc^{+/0}$ redox couple, at a scan rate of 100 mV s^{-1}, with increasing amounts of *p*-cyanoanilinium tetrafluoridoborate (2.5; 5; 10; 25 and 50 mM, light red – dark red).

4.2.3.3 Cyclic voltammetry of [Ni^{II}(dppe)Cl_2]

The electrochemical behavior of [Ni^{II}(dppe)Cl_2] was explored with CV in MeCN solutions containing nBu_4NPF_6 (0.1 M) as electrolyte, using a BDD working electrode. The cyclic voltammograms of [Ni^{II}(dppe)Cl_2] in MeCN showed several irreversible features (Figure 4.5a), the response in the first scan is different from the second and third scans. In the first scan, an irreversible reduction is observed ($E_{p,c}$ = −1.51 V vs $Fc^{+/0}$), which may be assigned to a one or two-electron reduction of the nickel(II) center (Figure 4.5a, dark blue trace). A series of oxidation events are observed upon scanning back to more positive potentials ($E_{p,a}$ = −1.34, −0.95, −0.87, −0.75, −0.50 V vs $Fc^{+/0}$). The second and third scan feature two new reduction events at more positive potentials than in the first scan ($E_{p,c}$ = −1.34 and −1.45 V vs $Fc^{+/0}$; Figure 4.5a, light blue traces).

Two irreversible reduction processes were reported to occur in cyclic voltammograms of [Ni^{II}(dppe)Cl_2] ($E_{p,c}$ = −1.00 and −1.55 V vs SCE) in a mixture of tetrahydrofuran and hexamethylphosphoramide (0.1 M nBu_4NBF_4).[16] The irreversible nature of the reduction events is ascribed to the dissociation of the chloride ions upon reduction, with formation of [Ni^{I}(dppe)Cl] and [Ni^{0}(dppe)].[16] Further chemical reactions of the reduced nickel species may limit reversibility on the CV timescale.[15] Upon re-oxidation of the nickel(0) and nickel(I) species, compounds such as [Ni^{II}(dppe)Cl(MeCN)]$^+$ and [Ni^{II}(dppe)$(MeCN)_2$]$^{2+}$ may be formed, or disproportionation may occur forming [$Ni^{II}$$(dppe)_2$]$^{2+}$. The new reduction events observed in the second and third scan may thus be assigned to any of these species.

The electrochemical behavior of [Ni^{II}(dppe)Cl_2] was also investigated in the presence of *p*-HOTs and diphenylacetylene (Figure 4.5b). Reduction of [Ni^{II}(dppe)Cl_2] in the presence of *p*-HOTs resulted in a new low intensity reduction process ($E_{p,c}$ = −0.9 V vs $Fc^{+/0}$) (Figure 4.5b, red trace). The low intensity reduction feature was followed by more reduction processes without clear peak potentials. The reduction feature of [Ni^{II}(dppe)Cl_2] ($E_{p,c}$ = −1.55

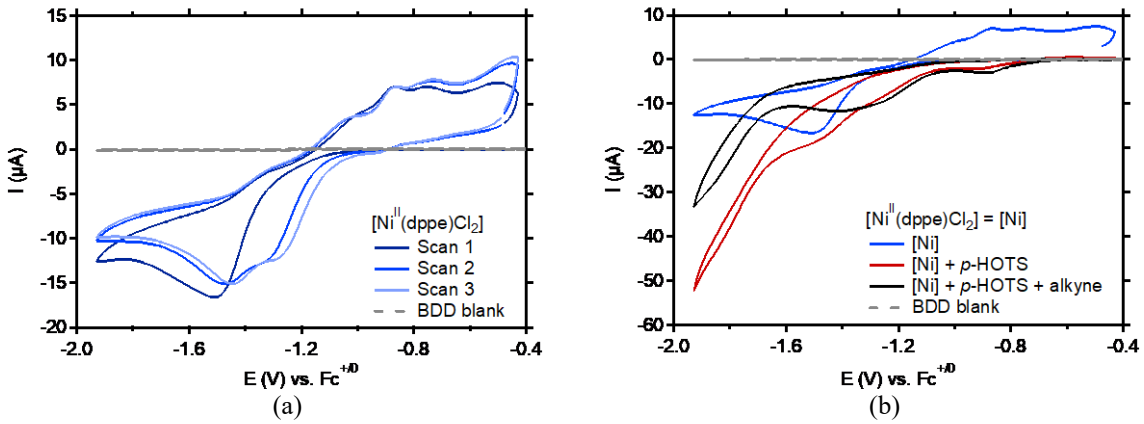

Figure 4.5. (a) Cyclic voltammograms of [Ni^{II}(dppe)Cl_2] (1.0 mM) in 0.1 M nBu_4NPF_6 in MeCN with a BDD WE, gold wire CE and Ag/AgCl RE externally referenced to the $Fc^{+/0}$ redox couple, at a scan rate of 100 mV s^{-1}. (b) Cyclic voltammograms of [Ni^{II}(dppe)Cl_2] (1.0 mM) from (a) (blue trace), and [Ni^{II}(dppe)Cl_2] in the presence of *p*-HOTs•H_2O (25 mM) (red trace), and [Ni^{II}(dppe)Cl_2] in the presence of both *p*-HOTs•H_2O (25 mM) and diphenylacetylene (25 mM) (black trace).

V vs $Fc^{+/0}$) was still visible to a certain degree, and was followed by another event likely associated with reduction of *p*-HOTs at the BDD surface.[33] A cyclic voltammogram recorded of [Ni^{II}(dppe)Cl_2] in the presence of *p*-HOTs and diphenylacetylene also featured the new low intensity reduction process ($E_{p,c}$ = −0.9 V vs $Fc^{+/0}$), followed by a second reduction with a clearer peak potential ($E_{p,c}$ = −1.40 V vs $Fc^{+/0}$; Figure 4.5b, black trace). A third reduction event was observed with an onset at −1.7 V vs $Fc^{+/0}$. No oxidation features were observed in the anodic scans.

4.2.4 Controlled-potential electrolysis experiments

4.2.4.1 CPE with [Ni^{II}(dppe)Cl_2] for electrocatalytic alkyne semi-hydrogenation

The complex [Ni^{II}(dppe)Cl_2] was studied for its activity as electrocatalyst for electrocatalytic semi-hydrogenation of methyl 3-phenyl-2-propynoate to methyl 3-phenyl-2-propenoate. Furthermore, the effect was studied of the addition of $[2(H)_2](PF_6)_3$ as a PCET mediator, which is discussed in Section 4.2.4.2. The electrocatalytic reactions were analyzed with ^{1}H NMR spectroscopy using an internal standard to determine conversion and yield.

A solution containing the complex [Ni^{II}(dppe)Cl_2] (1 mM), methyl 3-phenyl-2-propynoate (25 mM), and *p*-HOTs (50 mM) in MeCN was used in controlled-potential electrolysis (CPE) experiments at a potential of −1.30 V vs $Fc^{+/0}$, using a BDD working electrode and platinum counter electrode. The first CPE experiment resulted in formation of alkenes in 15% yield with an *E/Z* ratio of 1.8 (Table 4.1, entry 1); a representative ^{1}H NMR spectrum of the reaction mixture after workup is given in Figure A.4.17. However, replication of this experiment resulted in a significantly lower yield of 2% with an *E/Z* ratio of 1.0 (Table 4.1, entry 2). The working electrode was then changed from BDD to glassy carbon foam (RVC). Using an RVC electrode the yield of the reactions varied from 7 to 14% with *E/Z* ratios ranging between 0.6 and 1.1 (Table 4.1, entries 3−5). It was observed that the potential (E_{app} = –1.30 V vs $Fc^{+/0}$) was not stable during the electrocatalytic experiments with an RVC working electrode, and electrolysis was stopped when the potential started to drift to more positive potentials. Thus, changes in conversion and product yields may be due to different electrolysis times, as the drift in potential did not always occur after the same amount of time. The yields using the RVC electrode were similar to those obtained with the BDD system in a shorter

Table 4.1. Results of the electrocatalytic semi-hydrogenation of methyl 3-phenyl-2-propynoate with [Ni^{II}(dppe)Cl_2] as electrocatalyst.

Entry	Working electrode	Time (h)	Yield% (starting material %)	*E/Z* ratio	FE (%)
1	BDD	3	15 (48)	1.8	21
2	BDD	3	2 (79)	1.0	13
3	RVC	1.5	14 (73)	0.9	20
4	RVC	1.5	7 (63)	0.6	9
5	RVC	1.5	11 (49)	1.1	16

Reaction conditions: [Ni] = [Ni^{II}(dppe)Cl_2] (5 mM), *p*-HOTs•H_2O (50 mM), methyl 3-phenyl-2-propynoate (25 mM), nBu_4NPF_6 (0.1 M), MeCN, 3 h, E_{app} = –1.30 V vs $Fc^{+/0}$, an RVC or BDD (WE), Pt mesh (CE) and Ag/AgCl (RE) were used. Yield and *E/Z* ratio determined by NMR analysis with CH_2Br_2 as internal standard.

timespan (Table 4.1, entry 2). However, the *E/Z* selectivity of entry 1 could not be reproduced.

Significant variation in yield was observed for the experiments of entry 1 and 2 when a BDD electrode was used. The BDD electrode was electrochemically polished in an acidic solution with anodic polarization to ensure full oxidation of the surface before electrocatalytic experiments in order to diminish surface activity towards HER, as described previously.[44–46] Unfortunately, this was not sufficient to obtain reproducible results. Nevertheless, the results show that it is possible to perform the electrocatalytic semi-hydrogenation of methyl 3-phenyl-2-propynoate using $[Ni^{II}(dppe)Cl_2]$ as catalyst and *p*-HOTs as proton source in MeCN, although optimization of the reaction conditions should be explored.

4.2.4.2 CPE with $[Ni^{II}(dppe)Cl_2]$ and $[2(H)_2](PF_6)_3$

CPE experiments were also conducted using $[2(H)_2](PF_6)_3$ as mediator in the presence of the electrocatalyst $[Ni^{II}(dppe)Cl_2]$. The CPE experiment was performed at a potential of −1.30 V vs $Fc^{+/0}$ with a BDD working electrode and platinum counter electrode. It was hypothesized that in the presence of the mediator the potential might be more stable and that the yield and selectivity of the semi-hydrogenation reactions would be retained or possibly improved. CPE experiments in the presence of both $[2(H)_2](PF_6)_3$ (1 mM) and $[Ni^{II}(dppe)Cl_2]$ (5 mM) with methyl 3-phenyl-2-propynoate (25 mM), and *p*-HOTs (50 mM) resulted in 3% yield of methyl 3-phenyl-2-propenoate with an *E/Z* ratio of 1.0 (Table 4.2, entry 1). The yield of the reaction was 2% with an *E/Z* ratio of 2.5 when using equal concentrations of $[2(H)_2](PF_6)_3$ and $[Ni^{II}(dppe)Cl_2]$ (2 mM), with methyl 3-phenyl-2-propynoate (37.5 mM) and *p*-HOTs (100 mM) (Table 4.2, entry 2). A control experiment using $[Ni^{II}(dppe)Cl_2]$ (2 mM) in the absence of mediator resulted in a similar yield of 2% of alkene with an *E/Z* ratio of 2.5 (Table 4.2, entry 3). Formation of bubbles was observed at the electrode surface in experiments comprising $[2(H)_2](PF_6)_3$ indicating formation of dihydrogen gas, which is further discussed in Section 4.2.4.3.

Table 4.2. Results of the electrocatalytic semi-hydrogenation of methyl 3-phenyl-2-propynoate with $[Ni^{II}(dppe)Cl_2]$ as electrocatalyst and $[2(H)_2](PF_6)_3$ as mediator, and data from the literature.

Entry	[Co] in mM	[Ni] in mM	[H^+] in mM	Alkyne in mM	Time (h)	Yield% (starting material %)	*E/Z* ratio	FE (%)	Ref
1	1	5	50	25	3	3 (63)	1.0	16	this work
2	2	2	100	37.5	2	2 (93)	2.5	18	this work
3	0	2	100	37.5	2	2 (70)	2.5	12	this work
4[a]	2	2	100	37.5	not reported	14 (50)	not reported	14	[32]
5[a,b]	3	3	225	37.5	3	24 (74)	2.5	24	[32]

Reaction conditions: [Co] = $[2(H)_2](PF_6)_3$, [Ni] = $[Ni^{II}(dppe)Cl_2]$, *p*-HOTs•H_2O, methyl 3-phenyl-2-propynoate, nBu_4NPF_6 (0.1 M), MeCN, E_{app} = –1.30 V vs $Fc^{+/0}$, BDD (WE), Pt mesh (CE) and Ag/AgCl (RE) were used. Yield and *E/Z* ratio determined by NMR analysis with CH_2Br_2 as internal standard. [a] Co = $[1H]^{2+}$, Ni = $[Ni^{II}(dppe)Cl_2]$, *p*-HOTs•H_2O, methyl 3-phenyl-2-propynoate (37.5 mM), nBu_4NBF_4 (0.1 M), MeCN, time not reported, E_{app} = −1.30 V vs $Fc^{+/0}$, BDD (WE), Zn (CE), Ag/AgOTf (RE) were used.[32] [b] [Co] = $[1H]^{2+}$, [Ni] = $[Ni^{II}(dppe)Cl_2]$, *p*-HOTs•H_2O, $nBu_4N(NTf_2)$ (NTf_2^- = bis-trifluoromethanesulfonimidate; 75 mM), MeCN/DME (3:1).

Use of the PCET mediator $[1H]^{2+}$ (2 mM) in combination with $[Ni^{II}(dppe)Cl_2]$ (2 mM) in similar reaction conditions, was reported to yield 14% methyl 3-phenyl-2-propenoate, the *E/Z* ratio was not reported (Table 4.2, entry 4).[32] Optimization of this system by increasing the concentration of *p*-HOTs and use of a mixed solvent system MeCN/DME (3:1) resulted in an improved yield of 24% with an *E/Z* ratio of 2.5 (entry 5).[32] Compound $[1H]^{2+}$ used by the group of Peters seems to operate more efficiently than $[2(H)_2](PF_6)_3$ as mediator in the semi-hydrogenation reaction in combination with $[Ni^{II}(dppe)Cl_2]$.

The low Faradaic efficiencies observed in both our system and the system reported by the group of Peters (<25% FE to alkene)[32] are attributed to the occurrence of side reactions such as HER. The research described in this Chapter concerns reductive electrocatalytic processes for which a metal-hydride intermediate is essential. Nickel(I)-hydride and nickel(II)-hydride compounds are both active intermediates for hydrogenation of alkynes.[10] Metal-hydride compounds are also known intermediates for HER, which results in lower Faradaic efficiency.

Direct reduction of a nickel(II) compound to a nickel(0) intermediate in the presence of protons commonly results in generation of a nickel(II)-hydride intermediate.[7] However, at the operating potential this nickel(II)-hydride intermediate is often quickly reduced to a nickel(I)-hydride. Nickel(I)-hydride species are more active for HER, whereas nickel(II)-hydride compounds generally are not susceptible to protonation with subsequent formation of dihydrogen.[7,8,17]

Generation of nickel(II)-hydride intermediates is also possible through reduction in the presence of a PCET mediator. Through this approach a nickel(II)-hydride intermediate may be generated from a nickel(II) compound at a lower operating potential, circumventing formation of a nickel(I)-hydride compound. It is, however, essential that the PCET mediator is reduced at a more positive potential than the nickel(II) compound, otherwise reduction of the nickel(II)-hydride to the nickel(I)-hydride could still occur. The combination of an electrocatalyst with a mediator requires a close match in redox potentials of roughly 50 mV to provide optimal efficiency, although a larger difference is also possible.[19,47]

The condition of properly matching redox potentials was met for $[Ni^{II}(dmpe)_2]^{2+}$ in combination with $[1H]^{2+}$, for which the redox potentials differ by approximately 450 mV.[32] The unmediated electrocatalytic semi-hydrogenation reaction using only $[Ni^{II}(dmpe)_2]^{2+}$ at −1.75 V vs $Fc^{+/0}$ resulted in only trace amounts of alkene and approximately 73% FE towards formation of H_2.[32] However, in the presence of $[1H]^{2+}$ the semi-hydrogenation reaction proceeded at −1.30 V vs $Fc^{+/0}$, yielding 63% of alkene (63% FE, *E/Z* ratio 1.0) and 36% FE for H_2 formation.[32]

The compound $[Ni^{II}(dppe)Cl_2]$ in the presence of *p*-HOTs and alkyne showed redox activity at less negative potentials than $[Ni^{II}(dppe)Cl_2]$ in the absence of acid, as reported in Section 4.2.3.3. The reduction potential of the newly formed nickel species showed overlap with that of the mediator $[2(H)_2]^{3+}$. Based on the overlapping redox potentials of the electrocatalyst and the mediator $[2(H)_2]^{3+}$, it might be concluded that the semi-hydrogenation products are mainly a result of unmediated processes, and that no enhanced reactivity is observed in the presence

of the used mediator. To improve on this approach, either another nickel catalyst should be chosen with a more negative reduction potential or another mediator should be developed with a more positive reduction potential.

4.2.4.3 CPE using $[2(H)_2](PF_6)_3$ in presence of acid

In the semi-hydrogenation reaction in the presence of $[2(H)_2](PF_6)_3$, gas formation was observed at the BDD electrode surface, which was tentatively ascribed to formation of dihydrogen gas. CPE was performed using $[2(H)_2](PF_6)_3$ (1 mM) as potential HER electrocatalyst in MeCN in presence of *p*-HOTs (50 mM), using a BDD working electrode at a potential of −1.28 V vs $Fc^{+/0}$. The BDD electrode was pre-treated in an acidic environment with anodic polarization to ensure full oxidation of the BDD surface, a method frequently used to prepare the BDD for electrochemical measurements.[44–46]

$[2(H)_2](PF_6)_3$ in presence of *p*-HOTs indeed shows activity for HER on a BDD electrode, as evidenced by online monitoring of dihydrogen gas formation during the CPE experiment. Unfortunately, pre-treatment of the BDD electrode appeared not to be sufficient to completely shut down HER activity by the electrode, a large fraction of the observed dihydrogen production is due to activity of the BDD electrode under the employed conditions. After anodic pretreatment the electrode showed a significant lower activity towards HER on the CV timescale, but it slowly became more active over the duration of the CPE experiment (Figure A.4.19, black trace). Both current and dihydrogen gas production increased over time, indicating that the surface of the BDD electrode is reduced in the acidic environment, creating sites that are active for HER. A suitable acid and electrode material needs to be found in order to be able to determine the efficiency of $[2(H)_2](PF_6)_3$ as electrocatalyst for the formation of dihydrogen gas.

4.3 Conclusion

The new cobaltocenium complex $[2(H)_2](PF_6)_3$ was synthesized and characterized, and its redox activity in MeCN was investigated. Despite the presence of two pendant pyridyl groups that are readily protonated, $[2(H)_2](PF_6)_3$ is not effective as a PCET mediator with $[Ni^{II}(dppe)Cl_2]$ as electrocatalyst for the semi-hydrogenation of methyl 3-phenyl-2-propynoate under the conditions described in this Chapter. $[Ni^{II}(dppe)Cl_2]$ appeared to be a homogeneous electrocatalyst for the semi-hydrogenation of methyl 3-phenyl-2-propynoate also in the absence of a PCET mediator. $[2(H)_2](PF_6)_3$ might be a suitable electrocatalyst for the hydrogen evolution reaction, but unfortunately its catalytic activity could not be accurately determined due to the activity for HER of the working electrodes used in our study. Although $[2(H)_2](PF_6)_3$ appears to be not suitable as mediator for the electrocatalyst chosen in this Chapter, it might be a suitable PCET mediator for other reductive processes if the redox potentials are better matched.

4.4 Experimental

4.4.1 General information

All chemicals used were commercially purchased and used without any further purification. NaCp was either synthesized according to a known procedure,[48] or obtained from commercial vendors as a 2-3 M solution in THF. 2-Picolylcyclopentadiene,[34–36] and $LiCp^N$ were synthesized according to reported procedures.[36] *p*-Cyanoanilinium tetrafluoridoborate was synthesized according to a known procedure.[49] All reactions were carried out under nitrogen atmosphere using Schlenk techniques, unless when noted otherwise. Solvents were deoxygenated by three freeze-pump-thaw cycles and stored on molecular sieves. NMR spectra (^{1}H) were recorded on a Bruker AV 300, 400 or 500 MHz NMR spectrometer. Chemical shifts (δ) are reported in parts per million (ppm) using the residual solvent as internal standard. UV-vis spectra were recorded on a Varian Cary 50 scan spectrophotometer in a quartz cuvette with 1 cm path length. FT-IR spectra were recorded using a Perkin Elmer UATR Two spectrometer. An average of 4 scans was taken with a resolution of 4 cm^{-1}. ESI-MS measurements were performed using a Thermo Scientific MSQ plus or Shimadzu LCMS 2020 MS. The electrospray ionization (ESI-MS) method was employed, formic acid was added to the eluent with 1% final concentration. ESI-MS samples were prepared at a concentration of 1 mg/L in H_2O or MeCN. Elemental analyses were performed by Mikroanalytisches Laboratorium Kolbe in Oberhausen, Germany.

4.4.2 Crystal structure analysis

X-ray data collection and refinement were performed by Dr. M. A. Siegler at the Johns Hopkins University in Baltimore. Single crystals of $[2(H)_2](PF_6)_3$ suitable for X-ray analysis were grown by vapor diffusion of diethyl ether into a saturated acetone solution of the complex at room temperature. Crystallographic data are summarized in Table A.4.1. Reflection intensities were measured at 110(2) K using a SuperNova diffractometer (equipped with Atlas detector) with Mo Kα radiation (λ = 0.71073 Å) under the program CrysAlisPro (Version 1.171.36.32 Agilent Technologies, 2013). The same program was used to refine the cell dimensions and for data reduction. The structure was solved with the program SHELXS-2014/7 and was refined on F^2 with SHELXL-2014/7.[50] Numerical absorption correction based on gaussian integration over a multifaceted crystal model was applied using CrysAlisPro. The temperature of the data collection was controlled using the system Cryojet (manufactured by Oxford Instruments). The H atoms were placed at calculated positions (unless otherwise specified) using the instructions AFIX 23, or AFIX 43 with isotropic displacement parameters having values 1.2 U_{eq} of the attached C atoms. The H atom attached to N1 was found from difference Fourier map, and its coordinates were pseudofreely using the DFIX instruction in order to keep the N–H distance within an acceptable range. The structure of complex $[2(H)_2](PF_6)_3$ is ordered.

4.4.3 Electrochemistry

Metrohm Autolab PGSTAT 12 and 204 potentiostats were used in combination with NOVA 2.1 software for all electrochemistry experiments. Electrochemistry experiments for cyclic voltammetry were performed in a custom-made, glass, single-compartment three-electrode cell. The reference electrode was in contact with the electrolyte through a glass Luggin capillary. The cells and Luggin capillaries were cleaned if deemed necessary, based on the blank electrolyte measurements, by soaking them in a solution of 1 g/L (6.3 mM) $KMnO_4$ in 0.5 M H_2SO_4 overnight. The glassware was rinsed five times with Milli-Q water (>18.2 MΩ cm resistivity) to remove any $KMnO_4$ and soaked in diluted H_2SO_4 and H_2O_2 for 30 minutes. To get rid of any remaining H_2O_2 and acid, the glassware was rinsed five times with Milli-Q water. Finally, the glassware was boiled for 30 minutes in Milli-Q water three times before being oven-dried at 120 °C overnight.

The reference electrode used was a 3 M KCl Ag/AgCl electrode (Metrohm) for experiments in organic solvents. A flame-annealed, high-purity gold wire was used as the counter electrode in combination with a 3 mm (diameter) Metrohm Autolab glassy carbon (GC) or a 3 mm (diameter) Windsor Scientific boron-doped diamond (BDD) working electrode. For all electrochemistry measurements, a capacitor circuit was added between the electrolyte solution and the reference electrode to limit large oscillations in measured current.

The GC working electrode was prepared by polishing it twice for 1 minute on a Struers LaboPol-20 polishing machine with a silk Struers MD Dur 200 polishing pad at 200 RPM. The electrode was moved over the polish pad in a circular motion, opposite to pad rotation. For the first polish, a Struers DiaPro Dur 1 μm polish suspension was used. The second polish was done with a Struers OP-S NonDry 0.25 μm silica suspension. After polishing, the electrode was sonicated for 10 minutes in Milli-Q water. The BDD electrode was both physically and electrochemically polished before each measurement. The BDD electrode was polished with OPS for 1 minute at a speed of 200 RPM similar to the GC electrode. Following sonication in Milli-Q for 10 minutes the electrode was electrochemically polished by scanning the electrode between −1.0 V and +2.25 V vs. RHE for 100 cycles in 0.1 M aqueous sulfuric acid solution at a scan rate of 1 V s^{-1}. The electrode was then sonicated in Milli-Q for another 10 minutes to clean the electrode surface of any remaining sulfuric acid. After each polish a blank measurement of the electrode was performed, this often revealed some remaining signal in the first reductive scan, which was no longer present in later scans.

To negate any variations in potential between different Ag/AgCl reference electrodes, all measurements were related to the reversible $Fc^{+/0}$ couple. At the end of each experiment, 1 mg ferrocene was added to the electrolyte to function as an external standard, and a cyclic voltammogram was taken. From this cyclic voltammogram the $E_{1/2}$ of the $Fc^{+/0}$ couple was obtained, which was used as the reference potential.

Before electrochemical measurements, the solution containing the electrolyte was saturated with argon gas (Linde, Ar 5.0) for 30 minutes. To negate evaporation of solvent the argon gas was first bubbled through a wash bottle containing MeCN. During the measurement, the

argon flow was redirected over the solution to ensure an inert atmosphere. Between each measurement, the argon gas was bubbled through the electrolyte solution for at least 2 minutes. For all CV measurements, the starting potential of the CV was applied, immediately followed by the start of the CV staircase profile with a scan rate of 100 mV s^{-1} and a step size of 10 mV unless otherwise specified.

4.4.4 Controlled-potential electrolysis

Glassware was carefully cleaned as described in Section 4.4.3 and oven dried at 120 °C overnight before use. Controlled-potential electrolysis was performed in a divided cell separated by a cation exchange membrane (Solvay Aquivion® E98-15S - 20 mm diameter - RedoxMe). The working electrode consisted either of an RVC foam or BDD plate. RVC foam was obtained from Goodfellow (3000C Glassy Carbon (RVC) Foam – 6.35 × 150 × 150 mm – 96.5% porosity – 1.4 g/cm^3 density – 0.05 g/cm^3 bulk density) and cut to roughly these dimensions (20 × 5 mm), which was connected to a GC rod (Metrohm). The BDD plate was obtained from NeoCoat (BDD/Si 2500 ppm boron doping, 25 × 50 × 2 mm on both sides) and was isolated with PTFE tape to roughly these dimensions (25 × 4 mm). The BDD plate was polished through constant anodic polarization in a solution of AcOH (3 M) + H_2SO_4 (1 M) at 40 °C at a current density of 0.1 A/cm^2.[44–46] A platinum mesh counter electrode was flame annealed and rinsed with Milli-Q and MeCN before being placed in the solution. The reference electrode (LowProfile Ag/AgCl Reference - Equilabrium) was placed in the same compartment as the working electrode. The reference electrode was referenced against the $Fc^{+/0}$ couple before conducting a measurement. This was done by measuring a cyclic voltammogram of ferrocene (1 mg) in a different cell with a GC working electrode and a platinum wire as counter electrode.

For electrocatalytic experiments involving H_2 detection the following protocol was used: $[2(H)_2](PF_6)_3$ was dissolved in MeCN containing 0.1 M nBu_4NPF_6 and the solution was transferred to the cell to get a 1 mM concentration of catalyst, to this was added the proton source to get a 50 mM concentration of proton source. The solution was sparged with Ar for at least 15 minutes before starting the measurement. H_2 production was quantified using a Clark hydrogen electrode (Unisense H_2-NP). The Clark hydrogen electrode was calibrated by a five-time injection of a known amount of high-purity H_2 into the fully deaerated (30 min degassing with argon), thermostated (298 K) reactor (total volume 25.0 mL). For the electrocatalytic H_2 evolution experiments, the septum was punctured to get the needle of the Clark hydrogen electrode above the solution of the working electrode of the CPE to measure the headspace. Before starting the electrocatalytic experiment, a 30-minute period was taken to get a background H_2 measurement, after which the potential was applied and H_2 detection was started. The solution was stirred at 500 rpm during electrolysis. The potential applied (where $E_{cat/2}$) was taken from the cyclic voltammetry measurements and applied for 1 hour before stopping the electrolysis. Applied potential was E_{app} = −1.28 V vs $Fc^{+/0}$ for BDD WE with *p*-HOTs as proton source and E_{app} = −1.10 V vs $Fc^{+/0}$ for RVC WE with *p*-cyanoanilinium tetrafluoridoborate as proton source.

For electrocatalytic experiments involving alkyne semi-hydrogenation the following protocol was used: The mediator (if present) $[2(H)_2](PF_6)_3$, electrocatalyst $[Ni^{II}(dppe)Cl_2]$, alkyne substrate and proton source were dissolved in MeCN containing 0.1 M nBu_4NPF_6 and the solution was transferred to the cell resulting in concentrations of 1 or 2 mM $[2(H)_2](PF_6)_3$ (if present), 2 or 5 mM $[Ni^{II}(dppe)Cl_2]$, 25 or 37.5 mM substrate and 50 or 100 mM proton source. The solution was sparged with Ar for at least 15 minutes before starting the measurement. The solution was stirred at 500 rpm during electrolysis. The potential applied was taken from the cyclic voltammetry measurements (E_{app} = −1.30 V vs $Fc^{+/0}$), and applied for 3 hours before stopping the electrolysis, unless otherwise noted.

4.4.5 Workup procedure

After the electrolysis measurement, a workup was performed. The solution of the working electrode compartment was transferred to a round bottom flask, and the working electrode was rinsed with MeCN (2 × 1 mL), the working electrode compartment was also rinsed with additional MeCN (2 × 2 mL) to ensure full transfer of the contents of the electrolysis solution. The MeCN solvent was evaporated using a rotary evaporator, leaving a thick orange oil. To this was added Et_2O (20 mL) which results in formation of a precipitate of nBu_4NPF_6. The mixture was sonicated for 10 minutes. The mixture was filtered through a cotton plug into a separatory funnel to remove nBu_4NPF_6, the flask and cotton plug were washed with additional Et_2O (10 mL). To the separatory funnel was added saturated NH_4Cl solution (20 mL), and the organic fractions were extracted with Et_2O (5 × 20 mL). The combined Et_2O extracts were dried with anhydrous Na_2SO_4. The solution was filtered through a plug of cotton wool, the residual Na_2SO_4 was rinsed with additional Et_2O (3 × 15 mL) and the organic solvents were evaporated under reduced pressure to obtain a colorless to light-yellow oily residue.

4.4.6 Data analysis

The electrocatalytic H_2 evolution was calculated from the H_2 production data by converting the H_2 (data collected in µL) to µmol using the molar volume constant (1 mol of gas equals to 24.5 L).[51]

The alkyne conversion and alkene formation were performed by ^1H NMR analysis with an internal standard after CPE and workup. To the oily residue was added $CDCl_3$ (650 µL) and CH_2Br_2 (2.5 µL), and this was transferred to an NMR tube.

The Faradaic efficiency was calculated according to the following equation:

$$FE(\%) = \frac{nF(mol\ alkenes)}{total\ charge} * 100\%$$

Where *n* is assumed to be 2 for the two-electron process required to reduce the alkene from an alkyne and *F* is the Faraday's constant.

4.4.7 Synthetic protocols

Synthesis of [2]Cl

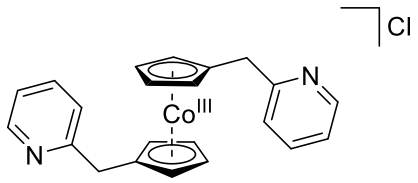

$LiCp^N$ (245 mg; 1.50 mmol) was dissolved in THF (3 mL) and the solution was cooled to –40 °C. To the cooled solution was added anhydrous $CoCl_2$ (98 mg; 0.75 mmol), the addition funnel was rinsed with THF (2 mL), the solution was allowed to come to room temperature and was stirred further overnight. The solvent was evaporated under reduced pressure to give a sticky dark purple residue. To the residue was added deionized water (20 mL) and a few drops of H_2O_2 (30% aqueous), and air was bubbled through the stirred solution for approx. 4 hours. The solution was filtered to obtain a dark orange filtrate. The aqueous solution was washed with diethyl ether (2 × 20 mL). The aqueous layer was collected, and the water was evaporated using a rotary evaporator. The product was taken up from the residue with chloroform until the extracts were colorless. The chloroform solution was filtered and after evaporation of the solvent a yellow viscous oil was obtained in a yield of 131 mg (36%). ^{1}H NMR [300 MHz, DMSO-d_6, 298 K] δ 8.52 (d, 2H), 7.79 (t, 2H), 7.39 (d, 2H), 7.30 (t, 2H), 5.72 (d, 4H), 5.68 (d, 4H), 3.96 (s, 4H); ESI-MS (H_2O): *m/z* (%) calcd: 371.1; found: 371.4 (100) $[M – Cl]^+$.

Synthesis of [2]PF_6

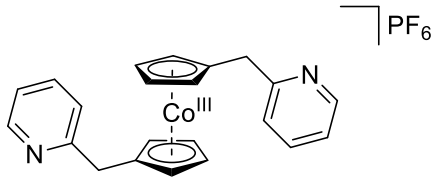

$AgPF_6$ (65 mg; 0.25 mmol) was added to a solution of [2]Cl (40 mg; 0.082 mmol) dissolved in MeCN (3 mL). After 1 hour stirring the solution was filtered to remove the AgCl, which was rinsed with additional MeCN. The filtrate was collected, and MeCN was evaporated under reduced pressure leaving a yellow residue of oily substance and solid. To this residue were added small amounts of chloroform to take up unreacted [2]Cl and the chloroform solution was filtered through a plug of Celite and rinsed with additional chloroform. To the solids that did not dissolve in chloroform was added acetone, which was able to dissolve [2]PF_6, the acetone solution was filtered through the plug of Celite used previously. The dark yellow acetone solution was layered with diethyl ether, which resulted in the formation of a yellow precipitate. The solvent was decanted, and the solids were transferred to a vial and dried further under vacuum. A yellow solid was obtained after drying with a yield of 15 mg (23%). ^{1}H NMR [300 MHz, DMSO-d_6, 298 K] δ 8.52 (d, 2H, =CH-N), 7.79 (td, 2H, =CH), 7.39 (d, 2H, =CH), 7.30 (t, 2H, =CH), 5.72, 5.68 (2 x t, 8H, C_5H_4), 3.96 (s, 4H, CH_2); ^{13}C NMR [75 MHz, DMSO-d_6, 298K] 157.6 (=C-N), 149.4 (=CH-N), 137.2 (=CH) 123.2 (=CH) 122.3 (=CH) 105.2 (C_5H_4), 84.7 (C_5H_4), 84.1 (C_5H_4), 35.3 (CH_2); ^{31}P {^{1}H} NMR [121.5 MHz, DMSO-d_6, 298 K] -144.25 (sept, PF_6); ESI-MS (MeCN): *m/z* (%) calcd: 371.1; found: 371.4 (100) $[M – PF_6]^+$.

Synthesis of $[2(H)_2](PF_6)_3$

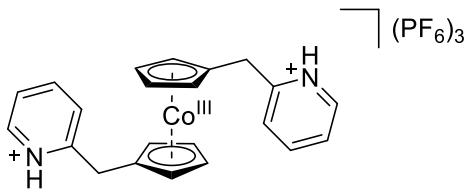

$LiCp^N$ (500 mg, 3.06 mmol, 2 eq.) was dissolved in anhydrous THF (25 mL) under N_2 atmosphere and the solution was cooled to –40 °C. Anhydrous $CoCl_2$ (198 mg, 1.54 mmol, 1.0 eq.) was suspended in THF (10 mL) and added to the ligand solution through canula transfer, and the reaction mixture was stirred at –40 °C for 15 min. The dark orange solution turned purple over time, after stirring for 20 h at RT, after which the solvent was removed *in vacuo*. To the sticky residue was added warm deionized water (50 mL) and a few drops of H_2O_2 (35% aqueous). Subsequently, the solution was exposed to 2 h of airflow, filtered and cooled down to 0 °C. The filtrate was washed with diethyl ether (25 mL) and the aqueous layer was decolorized with activated charcoal, filtered through celite and concentrated *in vacuo*. An aqueous 55% wt. HPF_6 solution (816 µL, 3.06 mmol, 2.0 eq.) was added slowly and the reaction mixture was kept in the refrigerator overnight. The resulting yellow precipitate was filtered, yielding $[2(H)_2](PF_6)_3$ as a yellow powder (112 mg, 0.13 mmol, 9%). ^{1}H NMR (500 MHz, CD_3CN) δ 8.61 (d, 2H, =CH-N), 8.53 (t, 2H, =CH), 7.95 (t, 2H, =CH), 7.83 (d, 2H, =CH), 5.83 (t, 4H, C_5H_4), 5.76 (t, 4H, C_5H_4), 4.31 (s, 2H, CH_2); ^{13}C NMR (126 MHz, CD_3CN) δ 152.85 (=C-N), 149.22 (=CH-N), 142.76 (=CH), 128.67 (=CH), 127.25 (=CH), 101.07 (C_5H_4), 87.10 (C_5H_4), 87.08 (C_5H_4), 32.00 (CH_2); ^{19}F NMR (471 MHz, CD_3CN) δ –72.04 - –73.54 (d, PF_6); ^{31}P NMR (202 MHz, CD_3CN) δ –144.16 (sept, PF_6). Elemental analysis: Calc. (%) for $C_{22}H_{22}CoN_2P_3F_{18}$ (MW = 808.00 g/mol): C: 32.68, H: 2.74, N: 3.46, found: (%) C: 32.66, H: 2.76, N: 3.45. FT-IR (neat, cm^{-1}): 465 (s), 477 (m), 514 (m), 555 (s), 744 (m), 773 (m), 816 (s), 933 (w), 1052 (w), 1173 (w), 1233 (w), 1254 (w), 1294 (w), 1328 (w), 1407 (w), 1432 (w), 1468 (w), 1543 (w), 1623 (m), 3125 (w), 3228 (w), 3320 (w), 3578 (w), 3646 (w). ESI-MS (MeCN): *m/z* (%) calcd: 371.1; found: 371.4 (100) $[M – 2H – 3PF_6]^+$.

Acknowledgements

Dr. Sipeng Zheng is gratefully acknowledged for performing the ESI-MS measurements. Dr. K.B. Sai Sankar Gupta is kindly thanked for his assistance with NMR measurements.

4.5 References

(1) Kusy, R.; Grela, K. Renaissance in Alkyne Semihydrogenation: Mechanism, Selectivity, Functional Group Tolerance, and Applications in Organic Synthesis. *Chem. Rev.* **2025**, *125* (9), 4397–4527. https://doi.org/10.1021/acs.chemrev.4c00001.

(2) Swamy, K. C. K.; Reddy, A. S.; Sandeep, K.; Kalyani, A. Advances in Chemoselective and/or Stereoselective Semihydrogenation of Alkynes. *Tetrahedron Lett.* **2018**, *59* (5), 419–429. https://doi.org/10.1016/j.tetlet.2017.12.057.

(3) Lindlar, H. Ein neuer Katalysator für selektive Hydrierungen. *Helv. Chim. Acta* **1952**, *35* (2), 446–450. https://doi.org/10.1002/hlca.19520350205.

(4) Nazmutdinov, R. R.; Dudkina, Y. B.; Zinkicheva, T. T.; Budnikova, Y. H.; Probst, M. Ligand and Solvent Effects on the Kinetics of the Electrochemical Reduction of Ni(II) Complexes: Experiment and Quantum Chemical Modeling. *Electrochim. Acta* **2021**, *395*, 139138. https://doi.org/10.1016/j.electacta.2021.139138.

(5) Vermaak, V.; Vosloo, H. C. M.; Swarts, A. J. The Development and Application of Homogeneous Nickel Catalysts for Transfer Hydrogenation and Related Reactions. *Coord. Chem. Rev.* **2024**, *507*, 215716. https://doi.org/10.1016/j.ccr.2024.215716.
(6) Pérez-García, P. M.; Moret, M.-E. Mechanistic Studies of the Oxidative Addition of Aryl Halides to Ni(0) Centers Bearing Phosphine Ligands. *CHIMIA* **2020**, *74* (6), 495–495. https://doi.org/10.2533/chimia.2020.495.
(7) Helm, M. L.; Stewart, M. P.; Bullock, R. M.; DuBois, M. R.; DuBois, D. L. A Synthetic Nickel Electrocatalyst with a Turnover Frequency Above 100,000 s-1 for H2 Production. *Science* **2011**, *333* (6044), 863–866. https://doi.org/10.1126/science.1205864.
(8) Wang, J.-W.; Liu, W.-J.; Zhong, D.-C.; Lu, T.-B. Nickel Complexes as Molecular Catalysts for Water Splitting and CO2 Reduction. *Coord. Chem. Rev.* **2019**, *378*, 237–261. https://doi.org/10.1016/j.ccr.2017.12.009.
(9) Eberhardt, N. A.; Guan, H. Nickel Hydride Complexes. *Chem. Rev.* **2016**, *116* (15), 8373–8426. https://doi.org/10.1021/acs.chemrev.6b00259.
(10) Fokin, I.; Kuessner, K.-T.; Siewert, I. Transition Metal Complex Catalyzed Photo- and Electrochemical (De)Hydrogenations Involving C=O and C=N Bonds. *Synthesis* **2021**, *54*, 295–314. https://doi.org/10.1055/a-1645-3254.
(11) Kaeffer, N.; Leitner, W. Electrocatalysis with Molecular Transition-Metal Complexes for Reductive Organic Synthesis. *JACS Au* **2022**, *2* (6), 1266–1289. https://doi.org/10.1021/jacsau.2c00031.
(12) Lin, Q.; Dawson, G.; Diao, T. Experimental Electrochemical Potentials of Nickel Complexes. *Synlett* **2021**, *32* (16), 1606–1620. https://doi.org/10.1055/s-0040-1719829.
(13) Bontempelli, G.; Fiorani, M.; Daniele, S.; Schiavon, G. An Electroanalytical Investigation on the Olefin Isomerization Reaction Promoted by Electrogenerated Cationic Nickel Hydrides. *J. Mol. Catal.* **1987**, *40* (1), 9–21. https://doi.org/10.1016/0304-5102(87)80002-0.
(14) Day, C. S.; Martin, R. Comproportionation and Disproportionation in Nickel and Copper Complexes. *Chem. Soc. Rev.* **2023**, *52* (19), 6601–6616. https://doi.org/10.1039/D2CS00494A.
(15) Bontempelli, G.; Magno, F.; Nobili, M. D.; Schiavon, G. Electroanalytical Investigation on Ligand-Disproportionation and -Exchange Equilibria in Nickel(II) and Nickel(I) Halide Phosphine Complexes in Acetonitrile. *J. Chem. Soc., Dalton Trans.* **1980**, *0* (11), 2288–2293. https://doi.org/10.1039/DT9800002288.
(16) Amatore, C.; Jutand, A. Activation of Carbon Dioxide by Electron Transfer and Transition Metals. Mechanism of Nickel-Catalyzed Electrocarboxylation of Aromatic Halides. *J. Am. Chem. Soc.* **1991**, *113* (8), 2819–2825. https://doi.org/10.1021/ja00008a003.
(17) Rountree, E. S.; Dempsey, J. L. Potential-Dependent Electrocatalytic Pathways: Controlling Reactivity with pKa for Mechanistic Investigation of a Nickel-Based Hydrogen Evolution Catalyst. *J. Am. Chem. Soc.* **2015**, *137* (41), 13371–13380. https://doi.org/10.1021/jacs.5b08297.
(18) Dey, S.; Masero, F.; Brack, E.; Fontecave, M.; Mougel, V. Electrocatalytic Metal Hydride Generation Using CPET Mediators. *Nature* **2022**, *607* (7919), 499–506. https://doi.org/10.1038/s41586-022-04874-z.
(19) Reid, A. G.; Machan, C. W. Redox Mediators in Homogeneous Co-Electrocatalysis. *J. Am. Chem. Soc.* **2023**, *145* (4), 2013–2027. https://doi.org/10.1021/jacs.2c10033.
(20) Connelly, N. G.; Geiger, W. E. Chemical Redox Agents for Organometallic Chemistry. *Chem. Rev.* **1996**, *96* (2), 877–910. https://doi.org/10.1021/cr940053x.
(21) Waniek, S. D.; Heine, C.; Zorn, D.; Lieberth, T.; Lauck, M.; Förster, C.; Heinze, K. Dicobaltocenium Amine–Proton, Electron, and H Atom Transfer. *Organometallics* **2022**, *41* (15), 2050–2058. https://doi.org/10.1021/acs.organomet.2c00211.
(22) Takebayashi, S.; Ariai, J.; Gellrich, U.; Kartashov, S. V.; Fayzullin, R. R.; Kang, H.-B.; Yamane, T.; Sugisaki, K.; Sato, K. Synthesis and Characterization of a Formal 21-Electron Cobaltocene Derivative. *Nat. Commun.* **2023**, *14* (1), 4979. https://doi.org/10.1038/s41467-023-40557-7.
(23) Prather, K. V.; Tsui, E. Y. Photoinduced Ligand-to-Metal Charge Transfer of Cobaltocene: Radical Release and Catalytic Cyclotrimerization. *Inorg. Chem.* **2023**, *62* (5), 2128–2134. https://doi.org/10.1021/acs.inorgchem.2c03779.
(24) Menia, D.; Pittracher, M.; Kopacka, H.; Wurst, K.; Neururer, F. R.; Leitner, D.; Hohloch, S.; Podewitz, M.; Bildstein, B. Curious Case of Cobaltocenium Carbaldehyde. *Organometallics* **2023**, *42* (5), 377–383. https://doi.org/10.1021/acs.organomet.2c00613.
(25) Kim, J.; Kim, J. H.; Ariga, K. Redox-Active Polymers for Energy Storage Nanoarchitectonics. *Joule* **2017**, *1* (4), 739–768. https://doi.org/10.1016/j.joule.2017.08.018.
(26) Magnoux, C.; Mills, D. P. Metallocene Anions: From Electrochemical Curiosities to Isolable Complexes. *Eur. J. Inorg. Chem.* **2022**, *2022* (11), e202101063. https://doi.org/10.1002/ejic.202101063.

(27) Ruth, J. C.; Milton, R. D.; Gu, W.; Spormann, A. M. Enhanced Electrosynthetic Hydrogen Evolution by Hydrogenases Embedded in a Redox-Active Hydrogel. *Chem. Eur. J.* **2020**, *26* (32), 7323–7329. https://doi.org/10.1002/chem.202000750.
(28) Ruth, J. C.; Schwarz, F. M.; Müller, V.; Spormann, A. M. Enzymatic Hydrogen Electrosynthesis at Enhanced Current Density Using a Redox Polymer. *Catalysts* **2021**, *11* (10), 1197. https://doi.org/10.3390/catal11101197.
(29) Koelle, U.; Infelta, P. P.; Graetzel, M. Kinetics and Mechanism of the Reduction of Protons to Hydrogen by Cobaltocene. *Inorg. Chem.* **1988**, *27* (5), 879–883. https://doi.org/10.1021/ic00278a026.
(30) Chalkley, M. J.; Del Castillo, T. J.; Matson, B. D.; Roddy, J. P.; Peters, J. C. Catalytic N2-to-NH3 Conversion by Fe at Lower Driving Force: A Proposed Role for Metallocene-Mediated PCET. *ACS Cent. Sci.* **2017**, *3* (3), 217–223. https://doi.org/10.1021/acscentsci.7b00014.
(31) Chalkley, M. J.; Oyala, P. H.; Peters, J. C. Cp* Noninnocence Leads to a Remarkably Weak C–H Bond via Metallocene Protonation. *J. Am. Chem. Soc.* **2019**, *141* (11), 4721–4729. https://doi.org/10.1021/jacs.9b00193.
(32) Derosa, J.; Garrido-Barros, P.; Li, M.; Peters, J. C. Use of a PCET Mediator Enables a Ni-HER Electrocatalyst to Act as a Hydride Delivery Agent. *J. Am. Chem. Soc.* **2022**, *144* (43), 20118–20125. https://doi.org/10.1021/jacs.2c09786.
(33) McCarthy, B. D.; Martin, D. J.; Rountree, E. S.; Ullman, A. C.; Dempsey, J. L. Electrochemical Reduction of Brønsted Acids by Glassy Carbon in Acetonitrile-Implications for Electrocatalytic Hydrogen Evolution. *Inorg. Chem.* **2014**, *53* (16), 8350–8361. https://doi.org/10.1021/ic500770k.
(34) Liu, T.; Guo, M.; Orthaber, A.; Lomoth, R.; Lundberg, M.; Ott, S.; Hammarström, L. Accelerating Proton-Coupled Electron Transfer of Metal Hydrides in Catalyst Model Reactions. *Nat. Chem.* **2018**, *10* (8), 881–887. https://doi.org/10.1038/s41557-018-0076-x.
(35) Mrózek, O.; Vinklárek, J.; Růžičková, Z.; Honzíček, J. Indenyl Compounds with Constrained Hapticity: The Effect of Strong Intramolecular Coordination. *Eur. J. Inorg. Chem.* **2016**, *2016* (33), 5250–5264. https://doi.org/10.1002/ejic.201601029.
(36) Potter, G. D.; Baird, M. C.; Cole, S. P. C. A New Series of Titanocene Dichloride Derivatives Bearing Cyclic Alkylammonium Groups: Assessment of Their Cytotoxic Properties. *J. Organomet. Chem.* **2007**, *692* (16), 3508–3518. https://doi.org/10.1016/j.jorganchem.2007.04.024.
(37) Vanicek, S.; Kopacka, H.; Wurst, K.; Müller, T.; Schottenberger, H.; Bildstein, B. Chemoselective, Practical Synthesis of Cobaltocenium Carboxylic Acid Hexafluorophosphate. *Organometallics* **2014**, *33* (5), 1152–1156. https://doi.org/10.1021/om401120h.
(38) Brauer, G. In *Handbuch der Präparativen Anorganischen Chemie*; Ferdinand Enke Verlag: Stuttgart, Germany, 1981; pp 1848–1849.
(39) Philippopoulos, a. I.; Bau, R.; Poilblanc, R.; Hadjiliadis, N. Transition Metal Derivatives of a ((Dimethylamino)Ethyl)Cyclopentadienyl Ligand. Synthesis and Structures of Amino-Containing Cyclopentadienyl Derivatives of Cobalt(I) and -(III) Including Water-Soluble Compounds. *Inorg. Chem.* **1998**, *37* (19), 4822–4827. https://doi.org/10.1021/ic970740h.
(40) Ahmed, M. E.; Staples, R. J.; Cundari, T. R.; Warren, T. H. Electrocatalytic Ammonia Oxidation by Pyridyl-Substituted Ferrocenes. *J. Am. Chem. Soc.* **2025**. https://doi.org/10.1021/jacs.4c14483.
(41) Lauck, M.; Förster, C.; Heinze, K. *N* -Cobaltocenium Amide as Reactive Nucleophilic Reagent for Donor–Acceptor Bimetallocenes. *Organometallics* **2017**, *36* (24), 4968–4978. https://doi.org/10.1021/acs.organomet.7b00790.
(42) Chalkley, M. J.; Garrido-Barros, P.; Peters, J. C. A Molecular Mediator for Reductive Concerted Proton-Electron Transfers via Electrocatalysis. *Science* **2020**, *369* (6505), 850–854. https://doi.org/10.1126/science.abc1607.
(43) Derosa, J.; Garrido-Barros, P.; Peters, J. C. Electrocatalytic Reduction of C–C π-Bonds via a Cobaltocene-Derived Concerted Proton–Electron Transfer Mediator: Fumarate Hydrogenation as a Model Study. *J. Am. Chem. Soc.* **2021**, *143* (25), 9303–9307. https://doi.org/10.1021/jacs.1c03335.
(44) Duo, I.; Levy-Clement, C.; Fujishima, A.; Comninellis, C. Electron Transfer Kinetics on Boron-Doped Diamond Part I: Influence of Anodic Treatment. *J. Appl. Electrochem.* **2004**, *34* (9), 935–943. https://doi.org/10.1023/B:JACH.0000040525.76264.16.
(45) Brocenschi, R. F.; Irikura, K.; Wachter, N.; Swain, G. M.; Rocha-Filho, R. C. Electrochemical Surface Rehydrogenation of Boron-Doped Diamond Electrodes after Electrochemical Polishing. *Diamond Relat. Mater.* **2023**, *136*, 110008. https://doi.org/10.1016/j.diamond.2023.110008.
(46) Macpherson, J. V. A Practical Guide to Using Boron Doped Diamond in Electrochemical Research. *Phys. Chem. Chem. Phys.* **2015**, *17* (5), 2935–2949. https://doi.org/10.1039/C4CP04022H.
(47) Tamirat, A. G.; Guan, X.; Liu, J.; Luo, J.; Xia, Y. Redox Mediators as Charge Agents for Changing Electrochemical Reactions. *Chem. Soc. Rev.* **2020**, *49* (20), 7454–7478. https://doi.org/10.1039/D0CS00489H.

(48) Panda, T. K.; Gamer, M. T.; Roesky, P. W. An Improved Synthesis of Sodium and Potassium Cyclopentadienide. *Organometallics* **2003**, *22* (4), 877–878. https://doi.org/10.1021/om0207865.
(49) Appel, A. M.; DuBois, D. L.; Rakowski DuBois, M. Molybdenum−Sulfur Dimers as Electrocatalysts for the Production of Hydrogen at Low Overpotentials. *J. Am. Chem. Soc.* **2005**, *127* (36), 12717–12726. https://doi.org/10.1021/ja054034o.
(50) Sheldrick, G. M. Crystal Structure Refinement with SHELXL. *Acta Crystallogr., Sect. C:Cryst. Struct. Commun.* **2015**, *71* (1), 3–8. https://doi.org/10.1107/S2053229614024218.
(51) Klein, D. M.; Passerini, L.; Huber, M.; Bonnet, S. A Stable Alkylated Cobalt Catalyst for Photocatalytic H2 Generation in Liposomes. *ChemCatChem* **2022**, *14* (20), e202200484. https://doi.org/10.1002/cctc.202200484.

Appendix A.4

Table A.4.1. Crystal and structure refinement data for $[2(H)_2](PF_6)_3$.

Crystal data	**$[2(H)_2](PF_6)_3$**
Chemical formula	$C_{22}H_{22}CoN_2 \cdot 3(F_6P)$
M_r	808.25
Crystal system, space group	Triclinic, *P*-1
Temperature (K)	110
a, *b*, *c* (Å)	6.8951(2), 8.8691(3), 12.2165(4)
α, β, γ (°)	96.440(3), 104.81(3), 101.663(3)
V (Å^3)	696.65 (4)
Z	1
Radiation type	Mo *K*α
μ (mm^{-1})	0.93
Crystal size (mm)	0.34 × 0.13 × 0.08
Data collection	
Diffractometer	SuperNova, Dual, Cu at zero, Atlas
T_{min}, T_{max}	0.816, 0.947
No. of measured, independent and observed [$I > 2\sigma(I)$] reflections	10628, 3188, 2837
R_{int}	0.028
$(\sin \theta/\lambda)_{max}$ (Å^{-1})	0.650
Refinement	
$R[F^2 > 2\sigma(F^2)]$, $wR(F^2)$, S	0.036, 0.093, 1.06
No. of reflections	3188
No. of parameters	211
H-atom treatment	H-atom parameters constrained
$\Delta\rho_{max}$, $\Delta\rho_{min}$ (e Å^{-3})	0.51, –0.30

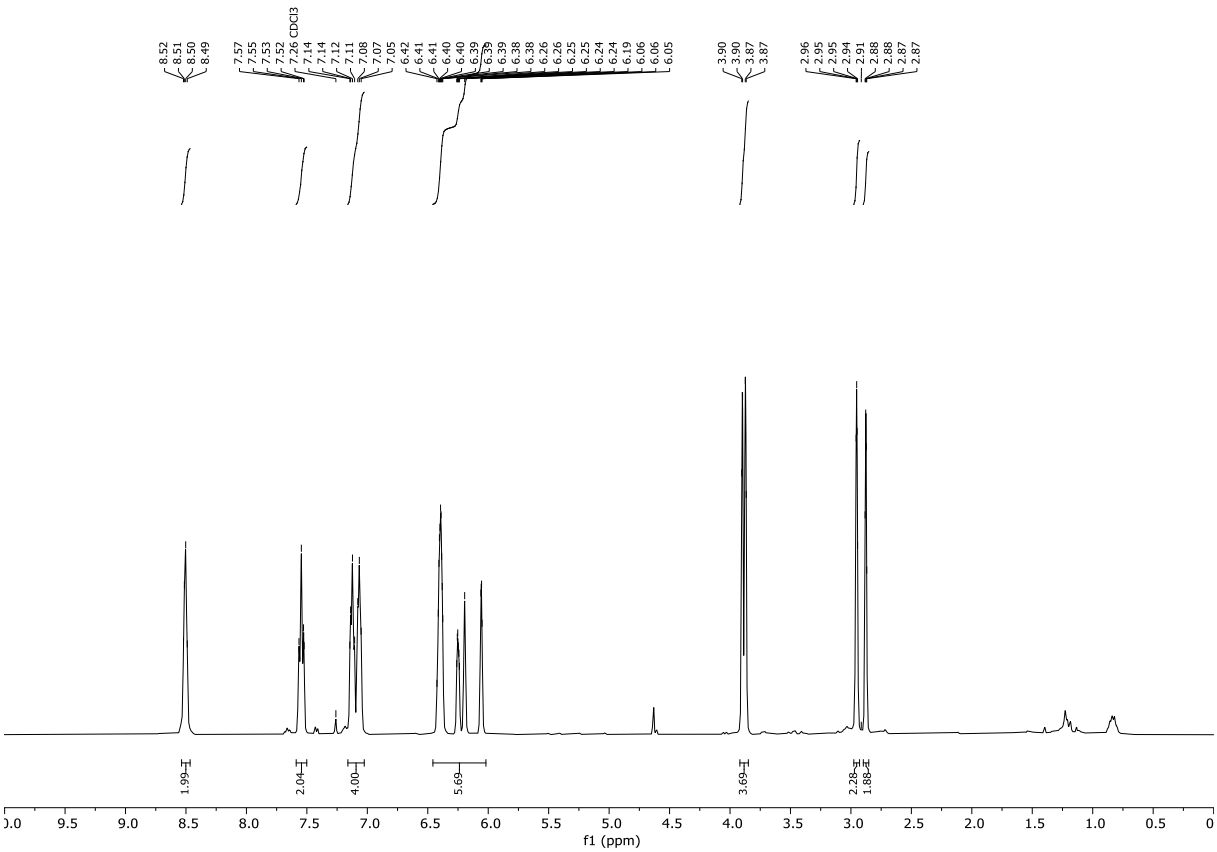

Figure A.4.1. ^{1}H NMR spectrum of (2-picolyl)cyclopentadiene tautomers (4) in $CDCl_3$.

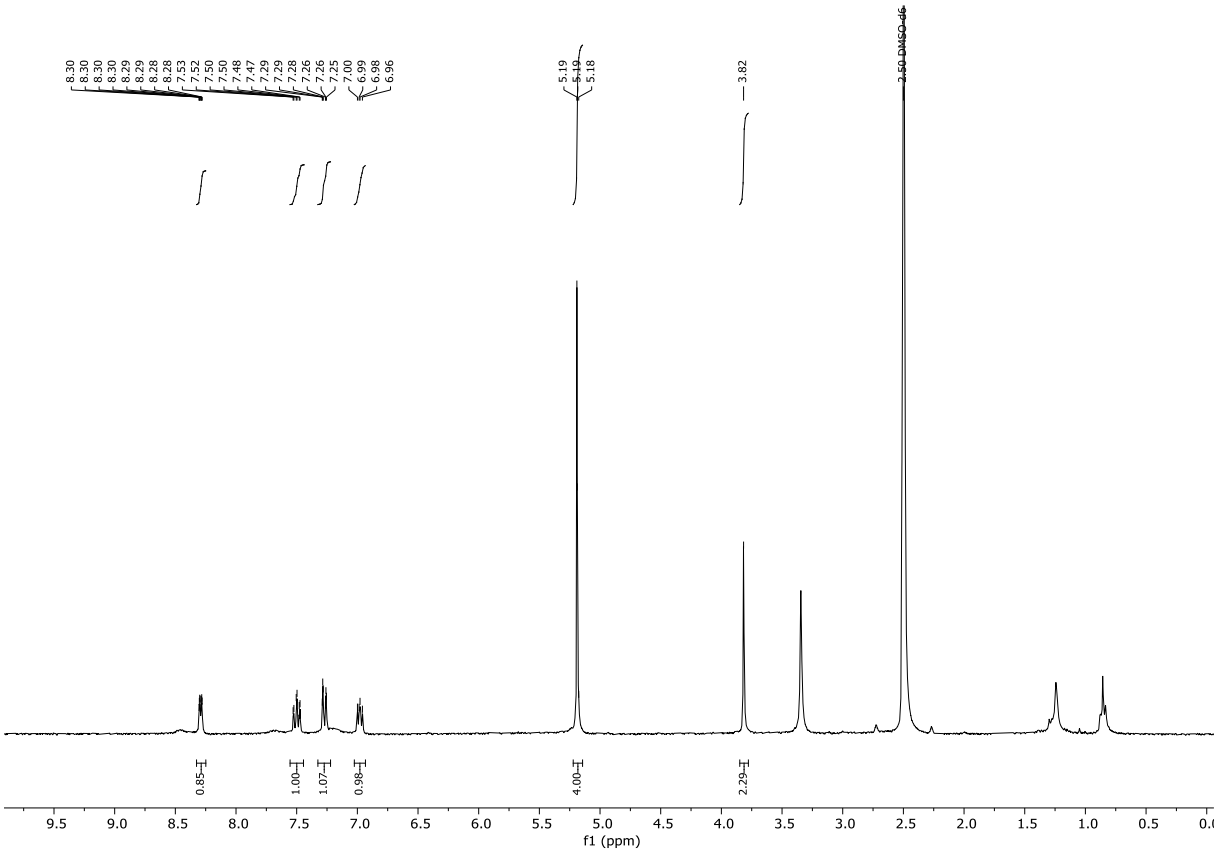

Figure A.4.2. ^{1}H NMR spectrum of $LiCp^{N}$ in DMSO-d_6.

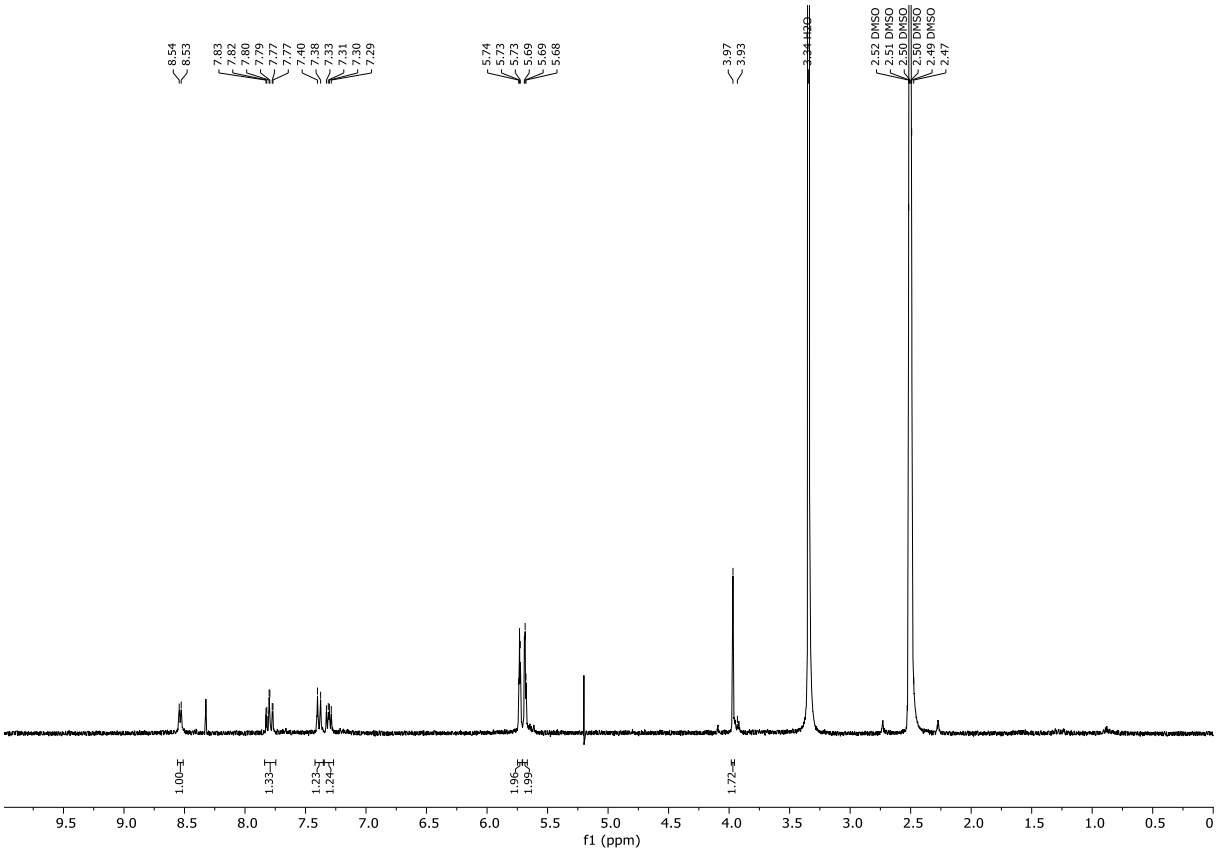

Figure A.4.3. ^{1}H NMR spectrum of [2]Cl in DMSO-d_6.

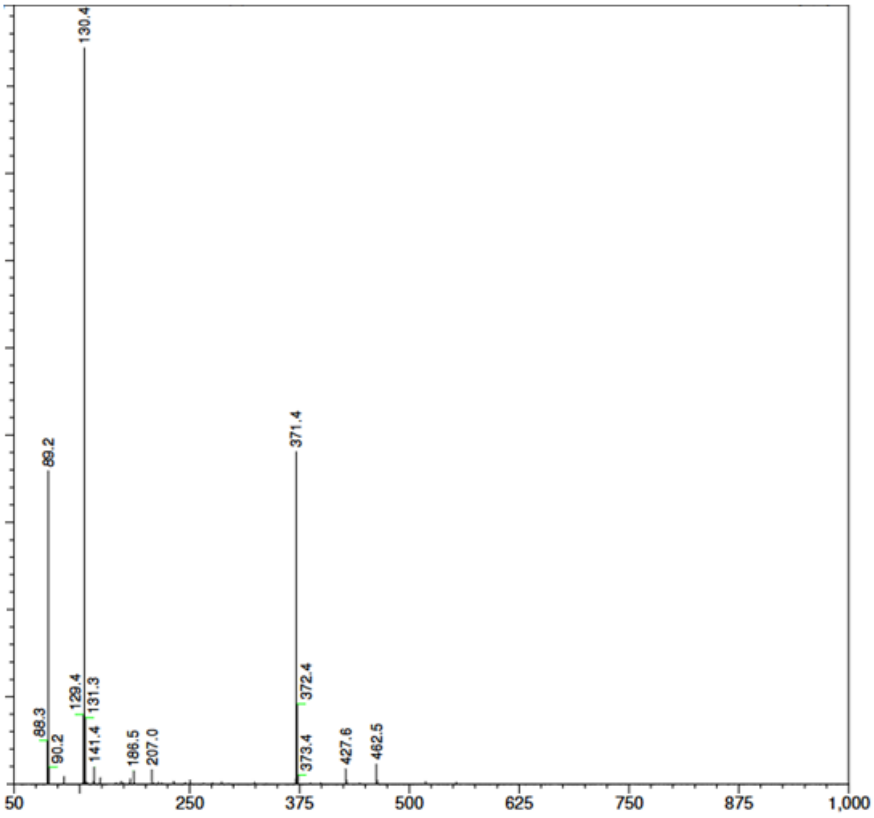

Figure A.4.4. ESI-MS spectrum of [2]Cl in H_2O. ESI-MS found (calcd.) for $[2]^+$ *m/z* 371.4 (371.10).

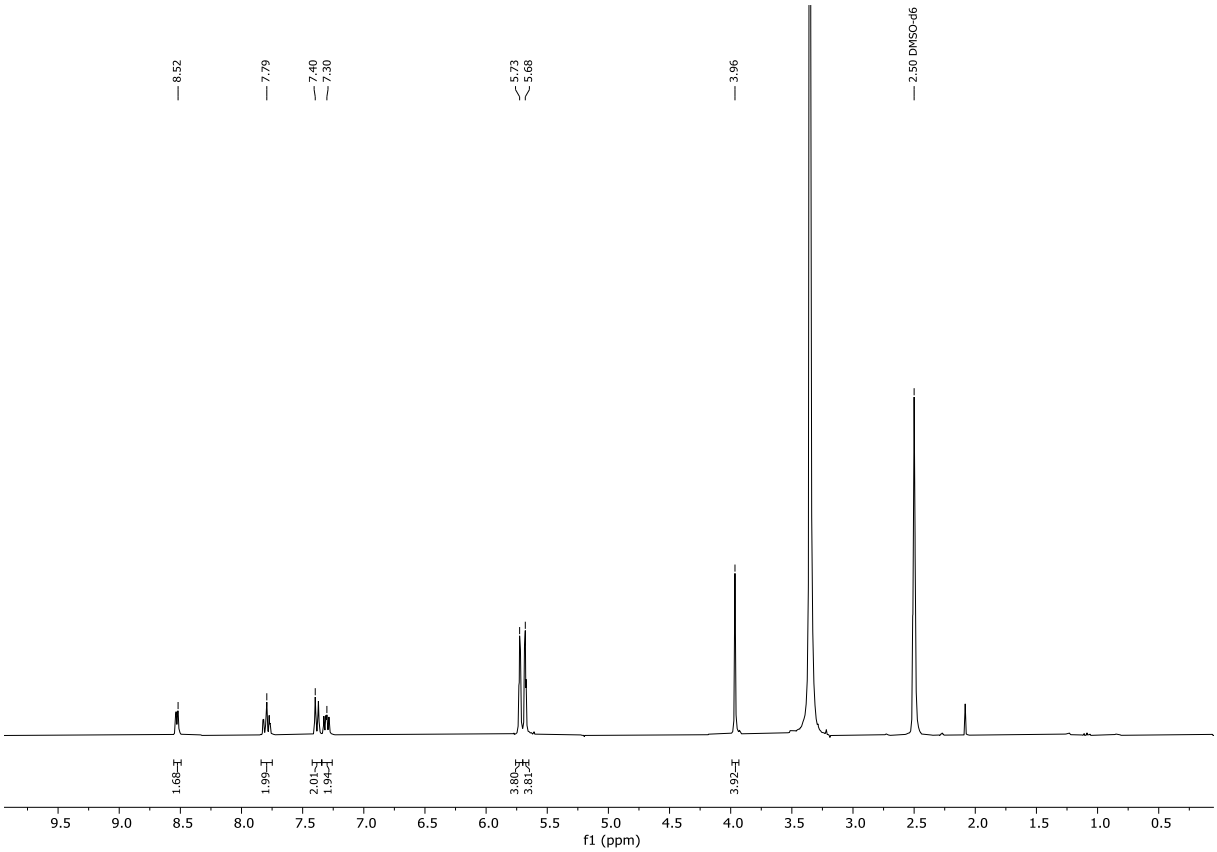

Figure A.4.5. ^{1}H NMR spectrum of [2]PF_6 in DMSO-d_6.

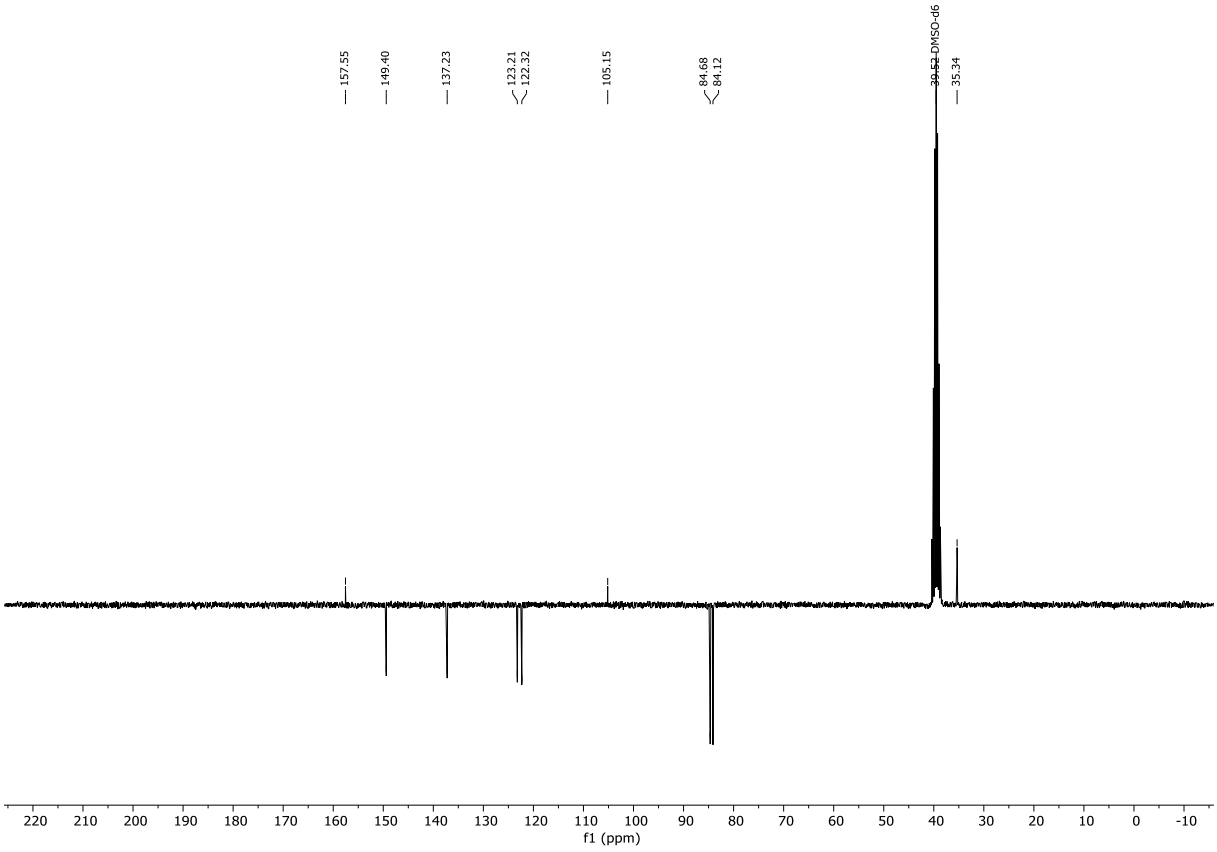

Figure A.4.6. ^{13}C NMR spectrum of [2]PF_6 in DMSO-d_6.

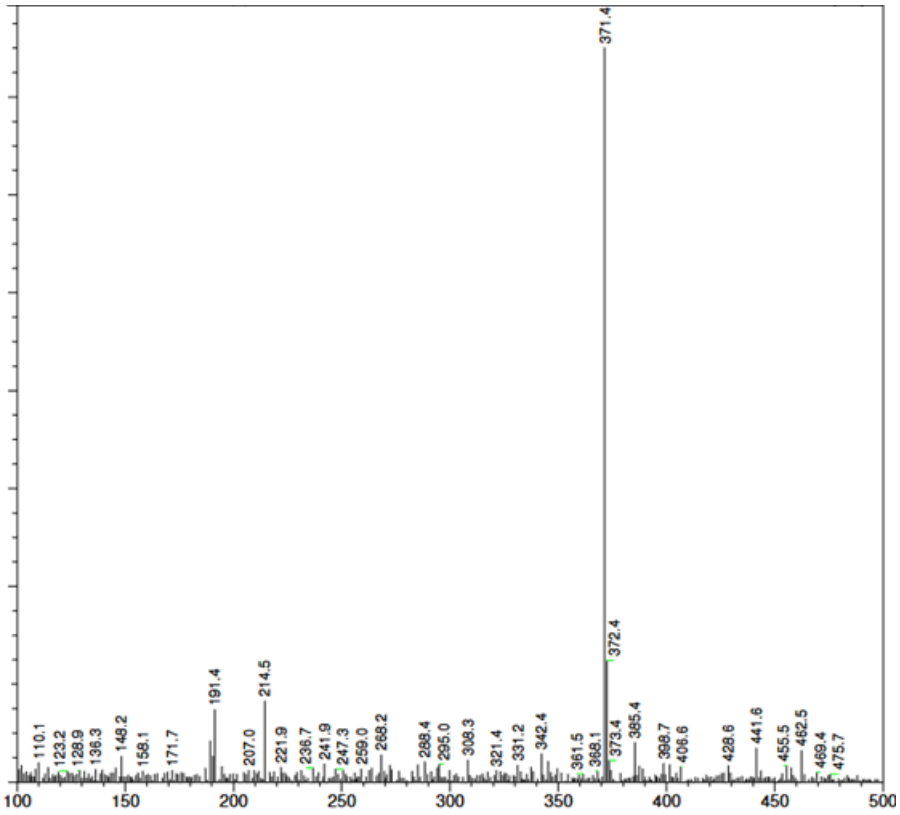

Figure A.4.7. ESI-MS spectrum of [2]PF_6 in MeCN. ESI-MS found (calcd.) for $[2]^+$ *m/z* 371.4 (371.10).

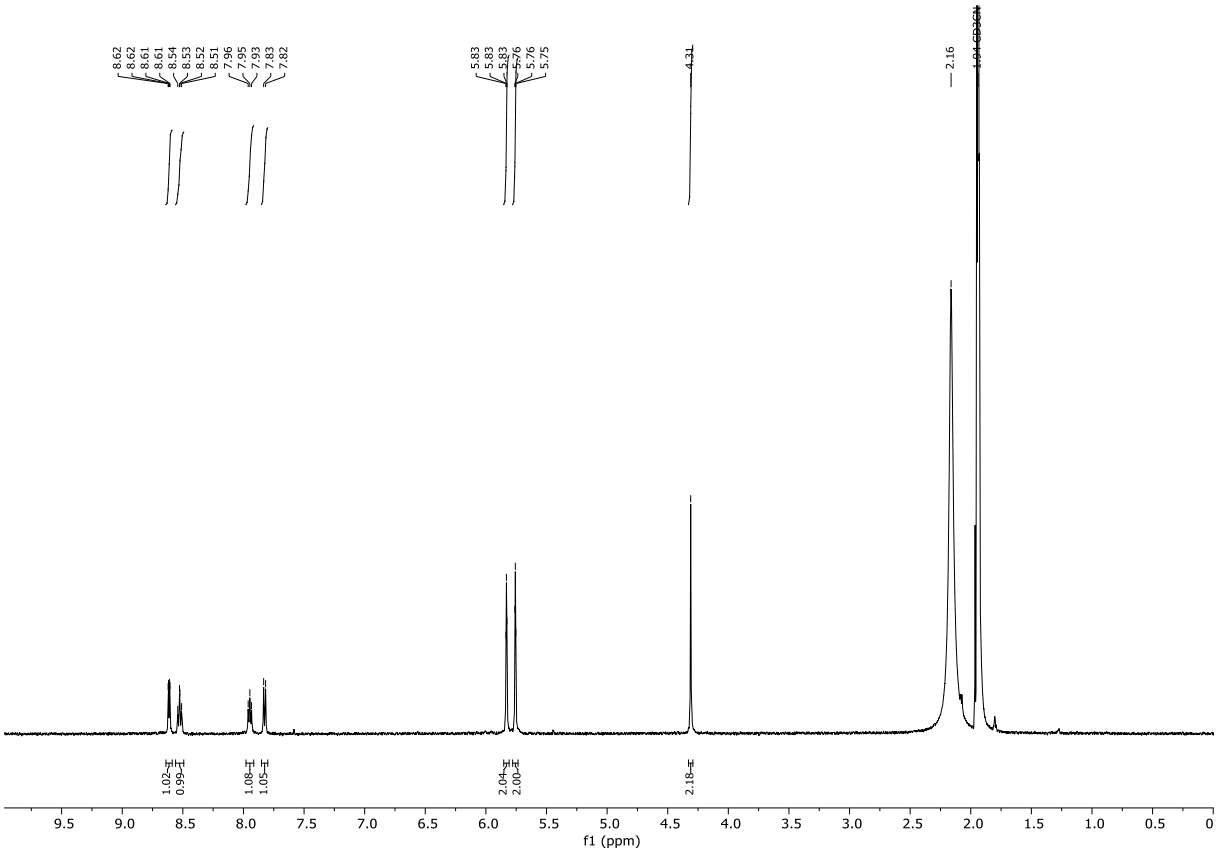

Figure A.4.8. ^1H NMR spectrum of $[2(H)_2](PF_6)_3$ in CD_3CN.

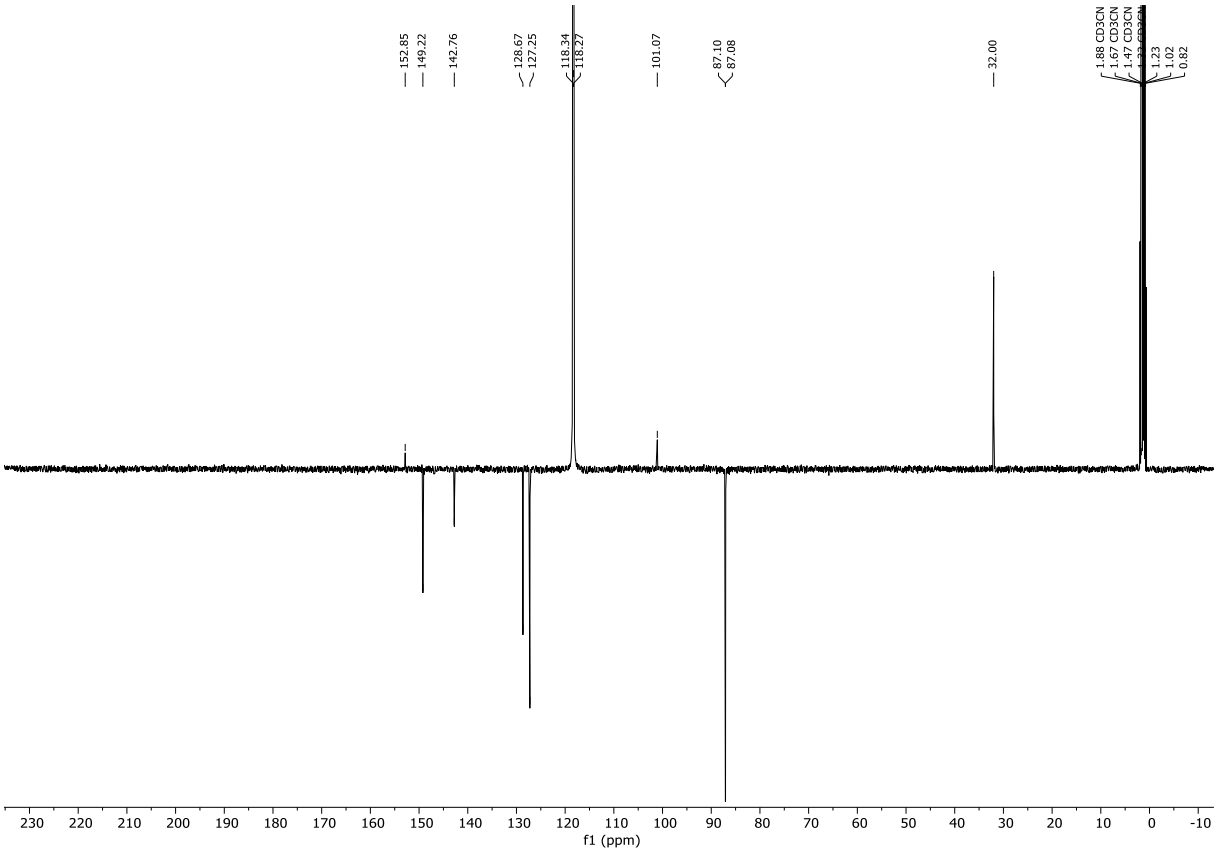

Figure A.4.9. ^{13}C NMR spectrum of $[2(H)_2](PF_6)_3$ in CD_3CN.

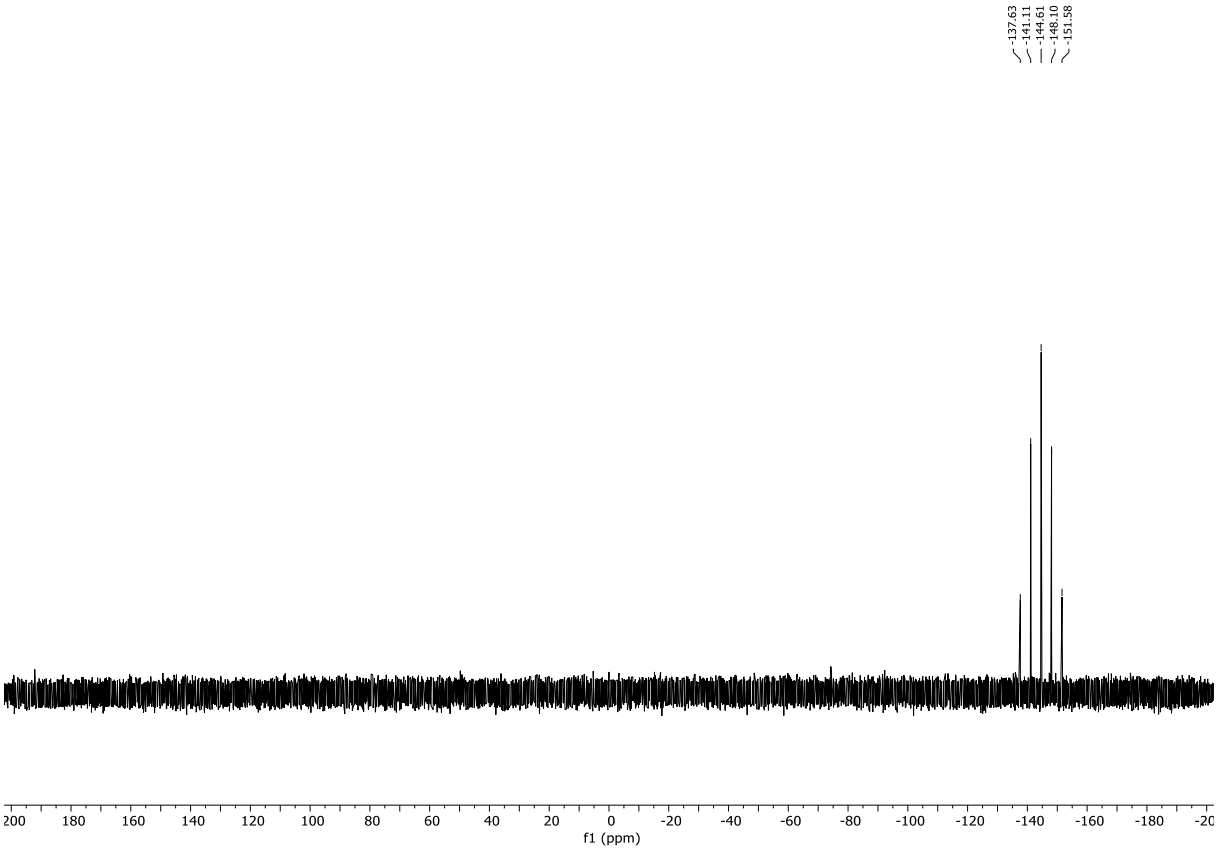

Figure A.4.10. ^{31}P NMR spectrum of $[2(H)_2](PF_6)_3$ in CD_3CN.

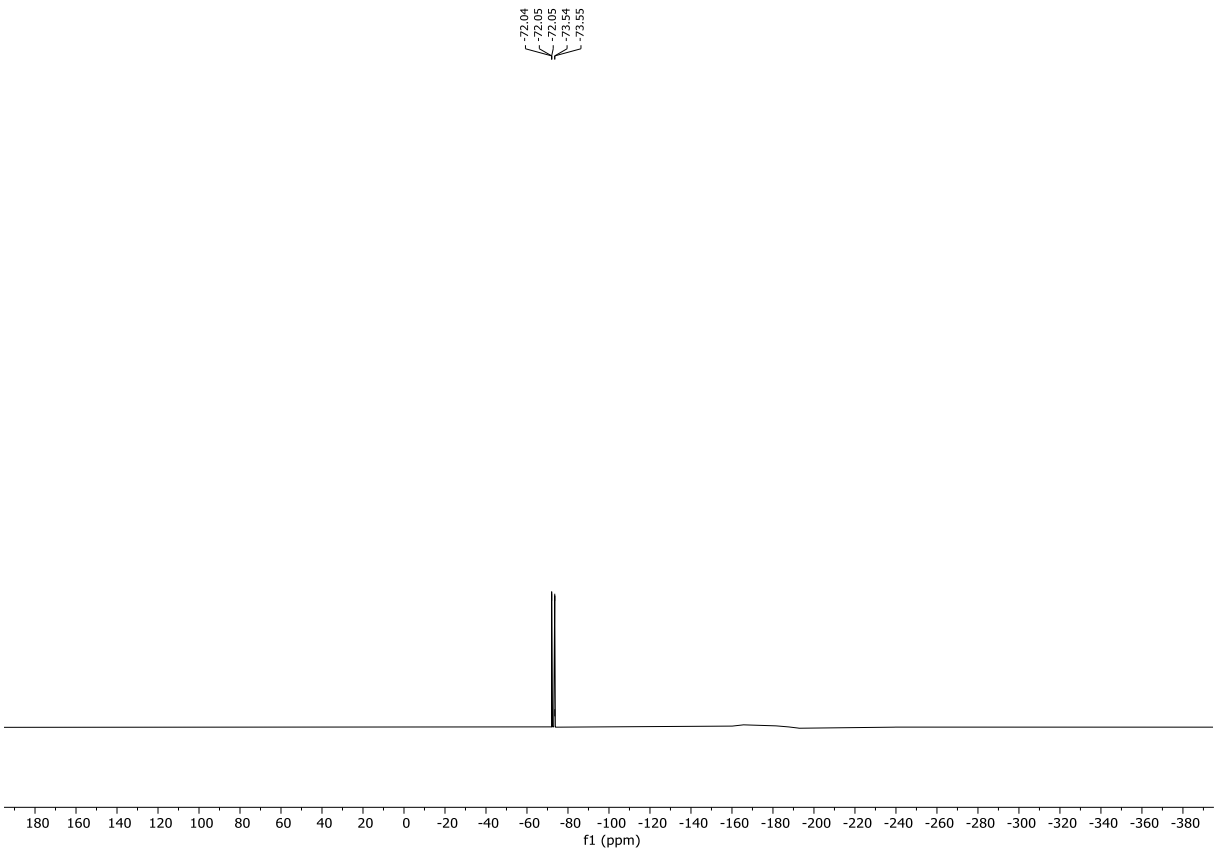

Figure A.4.11. ^{19}F NMR spectrum of $[2(H)_2](PF_6)_3$ in CD_3CN.

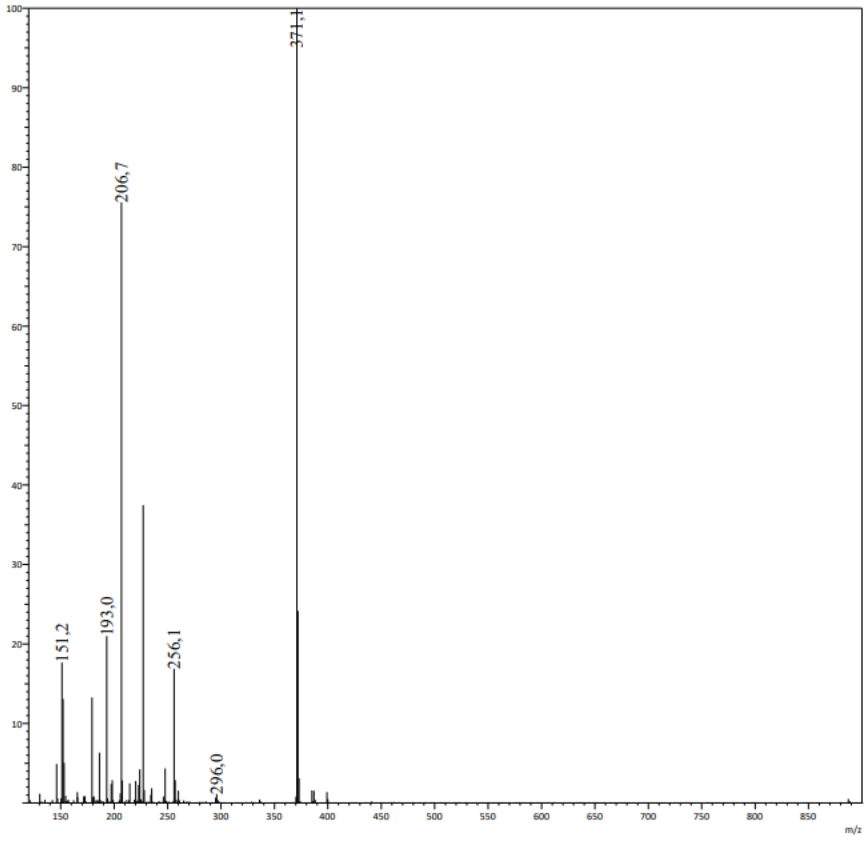

Figure A.4.12. ESI-MS spectrum of $[2(H)_2](PF_6)_3$ in MeCN. ESI-MS found (calcd.) for $[2]^+$ *m/z* 371.1 (371.10).

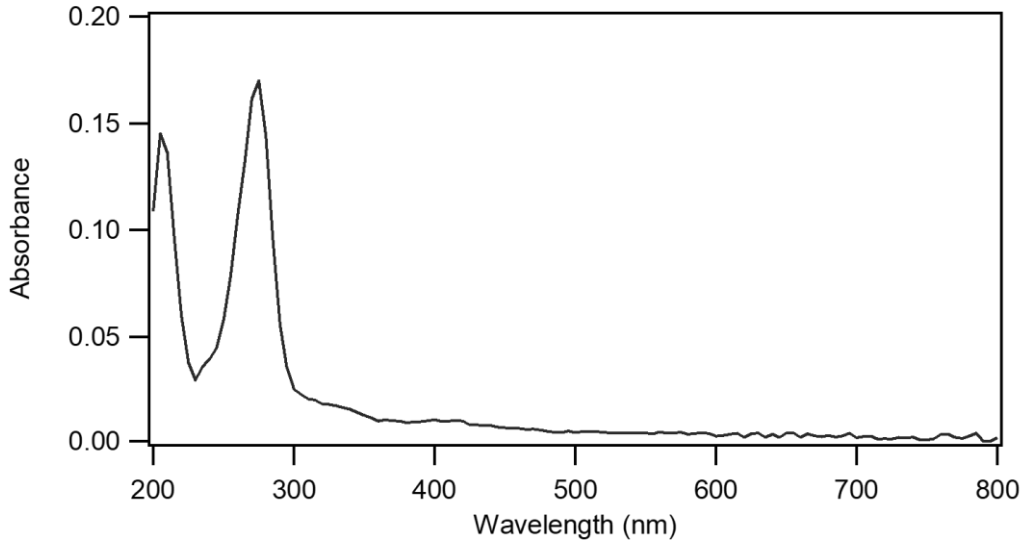

Figure A.4.13. UV-vis absorption spectrum of $[2(H)_2](PF_6)_3$ (4.17×10^{-6} M) in MeCN.

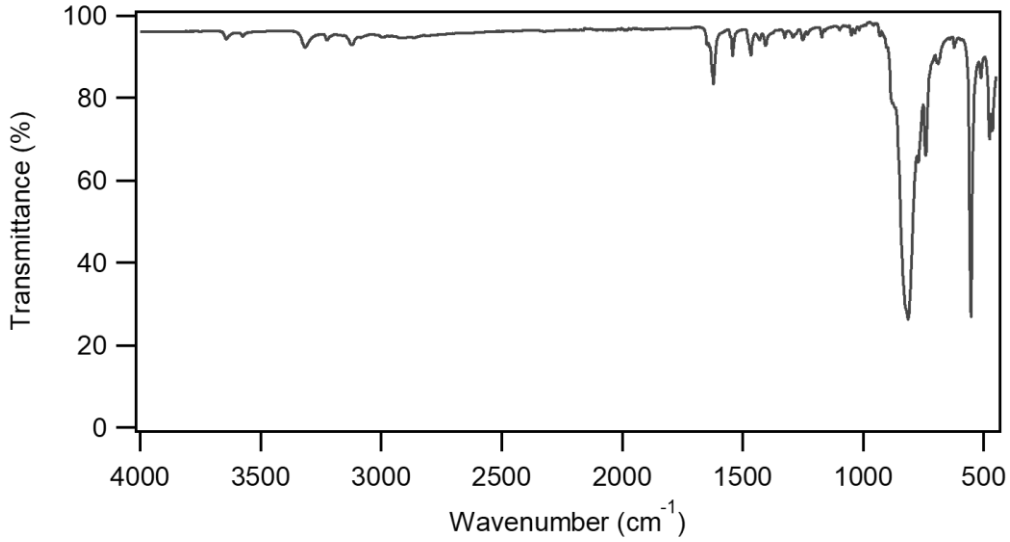

Figure A.4.14. FT-IR spectrum (neat) of $[2(H)_2](PF_6)_3$.

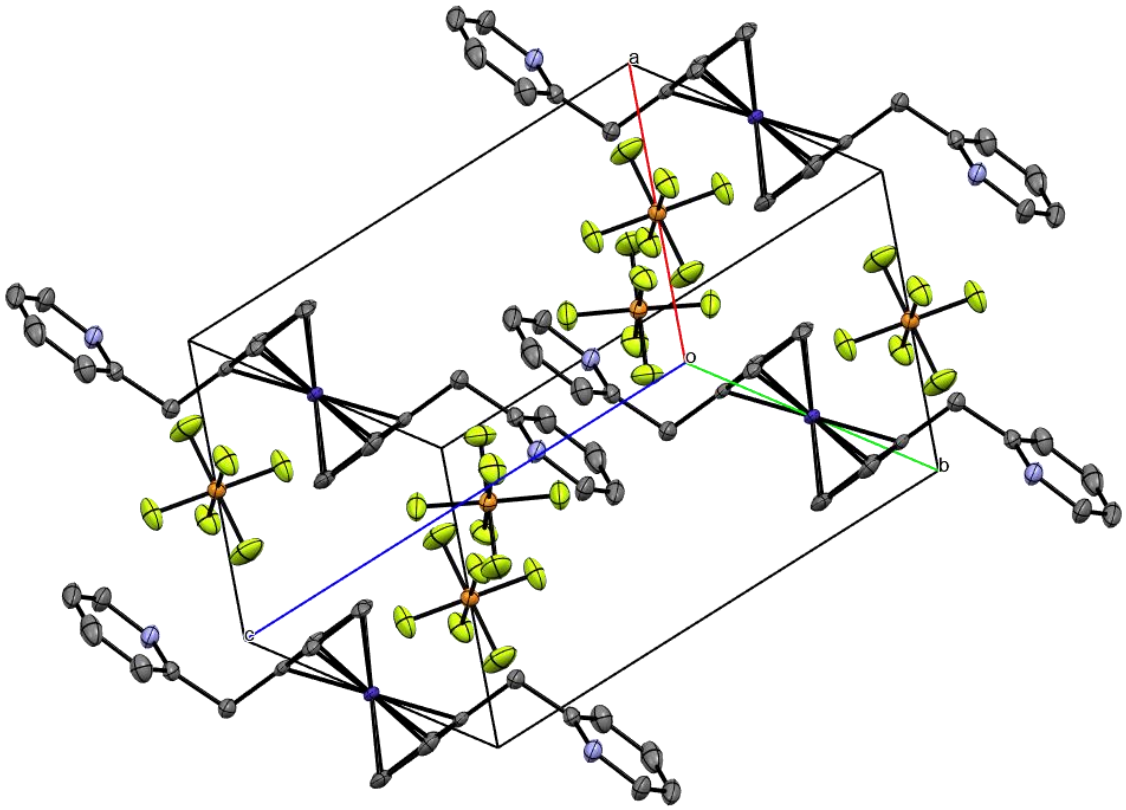

Figure A.4.15. Crystal packing of $[2(H)_2](PF_6)_3$.

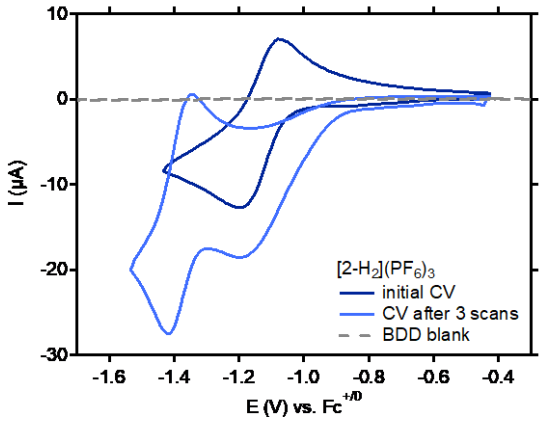

Figure A.4.16. Cyclic voltammogram traces of $[2(H)_2](PF_6)_3$ (1.0 mM) in 0.1 M nBu_4NPF_6 in MeCN with BDD WE, gold wire CE and Ag/AgCl RE, externally referenced to the $Fc^{+/0}$ redox couple, at a scan rate of 100 mV s^{-1}, first cyclic voltammogram taken after dissolution (dark blue), and after measuring the dark blue window three times (light blue). The cyclic voltammograms showcase loss of the proton and formation of $[2]^+$ with $E_{1/2}$ = –1.39 V vs $Fc^{+/0}$.

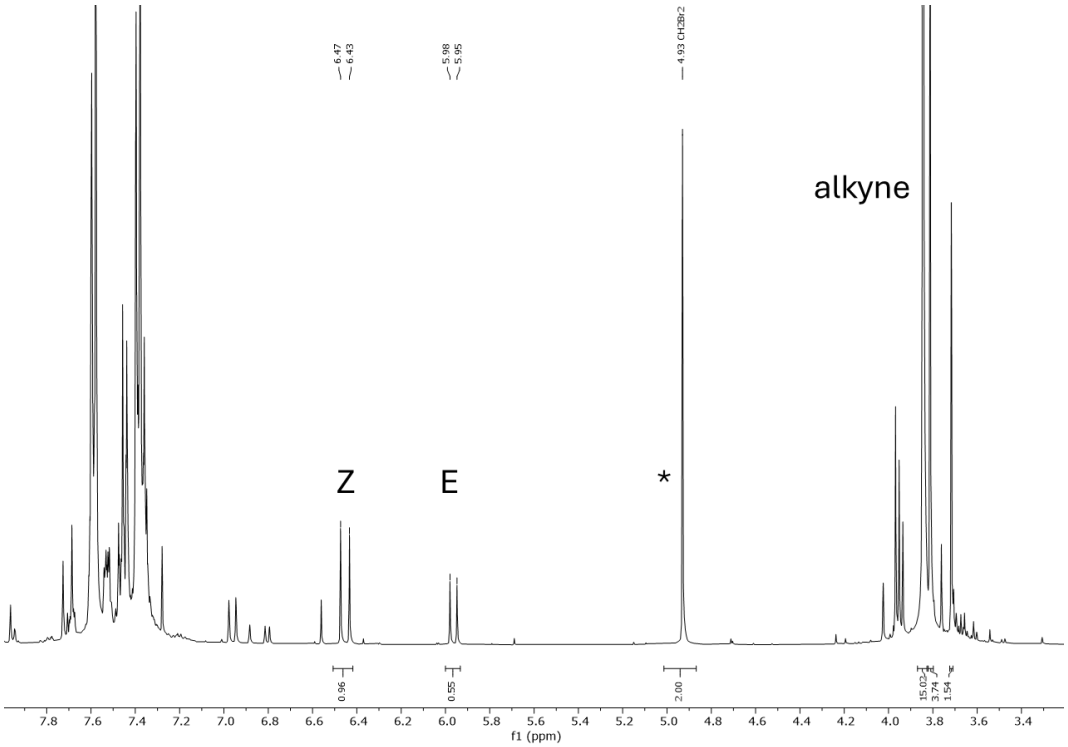

Figure A.4.17. ^{1}H NMR spectrum in $CDCl_3$ after CPE and work-up, with CH_2Br_2 as internal standard (*). Analysis after workup from CPE measurements of $[Ni^{II}(dppe)Cl_2]$ (5 mM) in 0.1 M nBu_4NPF_6 in MeCN with BDD WE, Pt mesh CE, Ag/AgCl RE, with *p*-HOTs•H_2O (50 mM), methyl 3-phenyl-2-propynoate (25 mM).

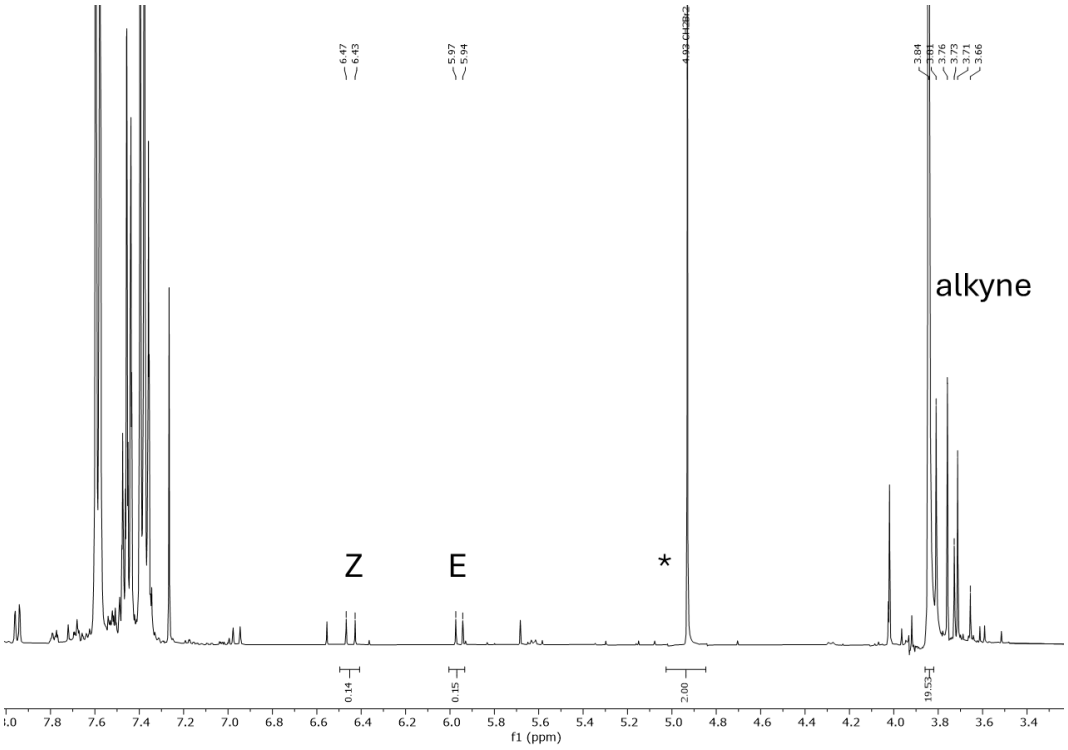

Figure A.4.18. ^{1}H NMR spectrum in $CDCl_3$ after CPE and work-up, with CH_2Br_2 as internal standard (*). Analysis after workup from CPE measurements of $[2(H)_2](PF_6)_3$ (1 mM) and $[Ni^{II}(dppe)Cl_2]$ (5 mM) in 0.1 M nBu_4NPF_6 in MeCN with BDD WE, Pt mesh CE, Ag/AgCl RE, with *p*-HOTs•H_2O (50 mM), methyl 3-phenyl-2-propynoate (25 mM).

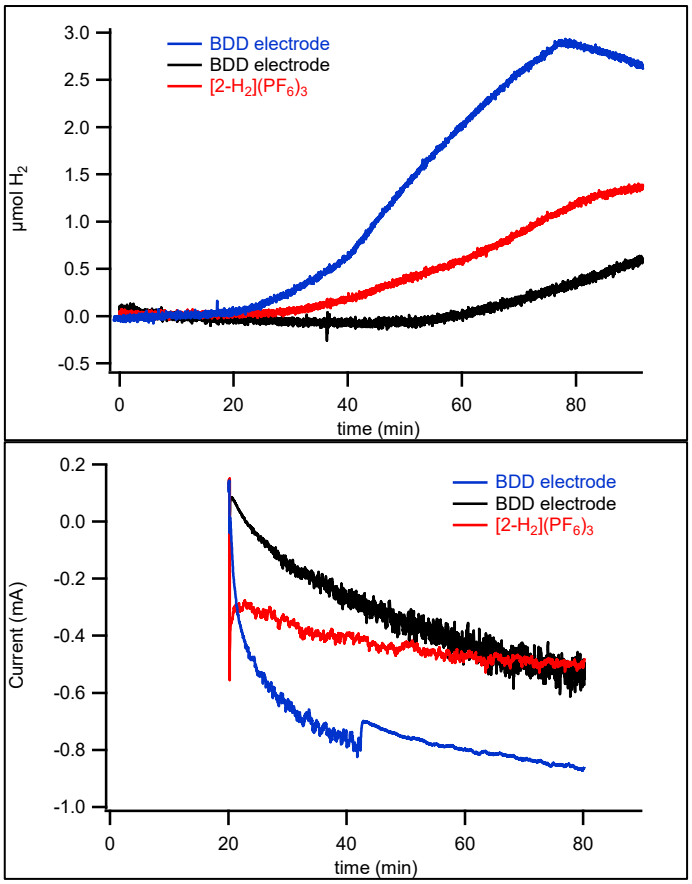

Figure A.4.19. Dihydrogen production (µmol H_2,top) and current (mA, bottom) during controlled-potential electrolysis with a BDD working electrode in the presence of *p*-HOTs (blue and black trace), and in the presence of $[2(H)_2](PF_6)_3$ (1 mM) (red trace). Reaction conditions: $[2(H)_2](PF_6)_3$ (1 mM), *p*-HOTs•H_2O (50 mM), nBu_4NPF_6 (0.1 M), MeCN, 1 h, E_{app} = –1.28 V vs $Fc^{+/0}$, BDD (WE), Pt mesh (CE) and Ag/AgCl (RE) were used. Two separate experiments (blue and black lines) of a BDD working electrode without $[2(H)_2](PF_6)_3$ showed increasing activity for dihydrogen production over time.

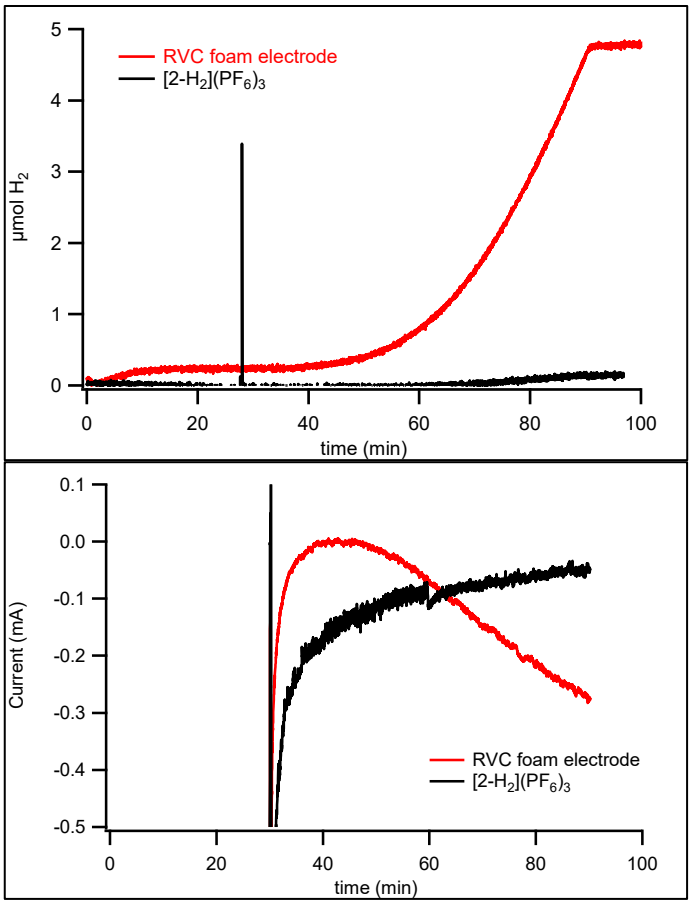

Figure A.4.20. Dihydrogen production (µmol H_2,top) and current (mA, bottom) during controlled-potential electrolysis with a RVC foam working electrode in the presence of *p*-cyanoanilinium tetrafluoridoborate (red trace), and in the presence of $[2(H)_2](PF_6)_3$ (1 mM) (black trace). Reaction conditions: $[2(H)_2](PF_6)_3$ (1 mM), *p*-cyanoanilinium tetrafluoridoborate (50 mM), nBu_4NPF_6 (0.1 M), MeCN, 1 h, E_{app} = –1.10 V vs $Fc^{+/0}$, RVC foam (WE), Pt mesh (CE) and Ag/AgCl (RE) were used.